



Description of the
multi-physics ice flow
model RIMBAY

M. Thoma et al.

RIMBAY – a multi-physics 3-D ice-dynamics model for comprehensive applications: model-description and examples

M. Thoma^{1,2}, K. Grosfeld¹, D. Barbi¹, J. Determann¹, S. Göller¹, C. Mayer², and
F. Pattyn³

¹Alfred Wegener Institute for Polar and Marine Research, Bussestrasse 24,
27570 Bremerhaven, Germany

²Bavarian Academy of Sciences, Commission for Glaciology, Alfons-Goppel-Str. 11,
80539 Munich, Germany

³Laboratoire de Glaciologie, Département des Sciences de la Terre et de l'Environnement
(DSTE), Université Libre de Bruxelles (ULB), CP 160/03, Avenue F.D. Roosevelt,
1050 Bruxelles, Belgium

Received: 30 May 2013 – Accepted: 5 June 2013 – Published: 19 June 2013

Correspondence to: M. Thoma (malte.thoma@awi.de)

Published by Copernicus Publications on behalf of the European Geosciences Union.

Title Page

Abstract

Introduction

Conclusions

References

Tables

Figures



Back

Close

Full Screen / Esc

Printer-friendly Version

Interactive Discussion



Abstract

Glaciers and ice caps exhibit currently the largest cryospheric contributions to sea level rise. Modelling the dynamics and mass balance of the major ice sheets is therefore an important issue to investigate the current state and the future response of the cryosphere in response to changing environmental conditions, namely global warming. This requires a powerful, easy-to-use, scalable multi-physics ice dynamics model. Based on the well-known and established ice sheet model of Pattyn (2003) we develop the modular multi-physics thermomechanic ice model RIMBAY, in which we improve the original version in several aspects like a shallow-ice–shallow-shelf coupler and a full 3-D-grounding-line migration scheme based on Schoof’s (2007) heuristic analytical approach. We summarise the Full–Stokes equations and several approximations implemented within this model and we describe the different numerical discretisations. The results are cross-validated against previous publications dealing with ice modelling, and some additional artificial set-ups demonstrate the robustness of the different solvers and their internal coupling. RIMBAY is designed for an easy adaption to new scientific issues. Hence, we demonstrate in very different set-ups the applicability and functionality of RIMBAY in Earth system science in general and ice modelling in particular.

1 Introduction

According to the Fourth Assessment Report (AR4) of the Intergovernmental Panel on Climate Change (IPCC) (IPCC, 2007) it is unequivocal, that Earth’s climate is warming since about 1850. This trend has been observed e.g., in rising air and ocean temperatures, in increased snow and ice melting, and in a rising sea level. According to more recent publications (e.g. Church et al., 2011; Rahmstorf et al., 2012) the trends estimated even for the worst scenarios of the AR4 are already reached or surpassed. Therefore, the imminent climate change will have profound impact on society.

GMDD

6, 3289–3347, 2013

Description of the multi-physics ice flow model RIMBAY

M. Thoma et al.

Title Page

Abstract

Introduction

Conclusions

References

Tables

Figures



Back

Close

Full Screen / Esc

Printer-friendly Version

Interactive Discussion



Description of the multi-physics ice flow model RIMBAY

M. Thoma et al.

Title Page

Abstract

Introduction

Conclusions

References

Tables

Figures

⏪

⏩

◀

▶

Back

Close

Full Screen / Esc

Printer-friendly Version

Interactive Discussion



However, none of the complex numerical Earth-System Models (ESMs) in the IPCC-report, used to compute the future climate trends, include the possible climate feedbacks of the large ice sheets in Greenland and Antarctica, resulting in a large uncertainty for the global mean sea-level predictions. These ice sheets play a crucial role in the Earth's hydrological cycle as they store about 75 % of the Earth's fresh water. In general, ice sheets accumulate mass from snow precipitation, which is compacted and finally transformed into ice. It follows the gravitational force and flows downhill from summits towards the ice sheet edges. However, this simplified view gets much more complex as different flow regimes exist within ice sheets (Fig. 1): the ice sheet's homogeneity is disturbed by Nunataks and fast flowing ice streams; at the base, subglacial lakes and a hydrological network alternates the basal boundary conditions of the ice sheet; and at the edges ice shelves interact with the ocean by massive melting and iceberg calving. Therefore, a numerical model has to deal with many different aspects of an ice sheet (and ice shelf) to represent its complex dynamic behaviour adequately and to improve future projections or hindcasts for palaeoclimatology.

During the last years great efforts have been undertaken to improve existing ice models and to incorporate them into coupled climate models (e.g., Rutt et al., 2009; Gillet-Chaulet et al., 2012; Levermann et al., 2012). Here, we present the **Revised Ice Model Based on frAnk pattYn**, the multi-physics ice sheet/ice shelf model RIMBAY. This model is originally based on the higher-order numerical ice-flow model of Pattyn (2003), which has been tested and applied to many scenarios (e.g. Pattyn, 2002, 2008, 2010; Pattyn et al., 2004). RIMBAY itself has been developed since 2009. Although the underlying Higher Order Model (HOM) and Full Stokes (FS)-physics remained basically unchanged, a Shallow Shelf Approximation (SSA) solver has been added to calculate the horizontally averaged velocities of ice streams and ice shelves. Additionally, the numerical solver implementation, the discretisation, the coupling between different solvers and the user interface has been improved in many aspects since it diverted from the original model. Keeping in mind that ice models have to deal with many different geophysical settings and boundary conditions, it is challenging to design a computer code

which is able to fulfill this needs for a large variety of users and applications. RIMBAY has been designed to be easy applicable to new scenarios, easy to extend and with clear interfaces to couple it with existing codes.

This paper is structured as follows: first, we clarify in Sect. 2 the sometimes imprecise usage of the term *model*, before we present in Sect. 3 the mathematical equations and several approximations founding the mathematical background of RIMBAY. Thereafter, we describe the numerical finite-difference implementation of these equations and how they can be solved with existing numerical solvers for linear differential equations in Sect. 4. Some more details about the code-implementation are given in Sect. 5, before we present some idealised example-applications of RIMBAY, with a main focus on cross-validation with previously published ice-model results and an example of internal code-coupling in Sect. 6. Finally, we demonstrate in Sect. 7 the wide spectrum of applications RIMBAY is already used for by several users.

2 Multi-physics ice sheet/shelf model RIMBAY

The term *model* is used in several ways in Earth system science, which can be confusing sometimes. Therefore, we first define what we understand as *model*, or to be more precise between which types of *model* we distinguish:

- Equations form the *mathematical model* describing the fundamental relationship between the relevant values of interest (e.g., velocity, temperature, and viscosity). In our context, these equations are mostly coupled differential equations which can not be solved analytically.
- These equations are solved with a computer, which requires a discretisation of the equations. This can be done in several distinct ways, depending on the demand of accuracy, stability, convergence properties, and resources (memory usage and computational coast). We refer to this as the *numerical model*.

Description of the multi-physics ice flow model RIMBAY

M. Thoma et al.

Title Page

Abstract

Introduction

Conclusions

References

Tables

Figures



Back

Close

Full Screen / Esc

Printer-friendly Version

Interactive Discussion



Description of the multi-physics ice flow model RIMBAY

M. Thoma et al.

Title Page

Abstract

Introduction

Conclusions

References

Tables

Figures

⏪

⏩

◀

▶

Back

Close

Full Screen / Esc

Printer-friendly Version

Interactive Discussion



- This numerical model has to be translated into a computer language (mostly a high-level programming language like Matlab, Fortran, C, or C++). It is common sense to refer to this computer programme as model, too. We use the expression *code* or the *implementation* to specify the lines forming this (sometimes compiled binary) programme.
- Finally, the code is applied to answer a specific scientific question (e.g. the contribution to sea level rise) of a specific domain (e.g., whole Antarctica or a subregion like the area of the Pine Island Glacier), or to study processes (e.g. the impact of basal water on ice dynamics) and the sensitivity to parameters or boundary conditions (e.g. geothermal heat flux, bedrock topography or ice thickness distribution). These applications of a computer programme are often called *model*, too. We refer to these applications as *experiments* or *scenarios*.

In general, we use the term RIMBAY for the implementation of the discretised equation, and therefore the compiled binary code, which includes not only the mathematical model, but also a sophisticated command-line interpreter and input–output interfaces for an easy usage. RIMBAY is distributed with a suit of example- and reference-scenarios and several additional programmes (mainly based on the bash-script language) providing several options to visualize the computed results with the Generic Mapping Tools (GMT, Wessel and Smith, 1998). In the following sections, we elaborate on these different model types and how they are used in RIMBAY.

3 Mathematical model

The mathematical field equations are based upon the conservation of mass, momentum, and energy

$$\frac{\partial \rho}{\partial t} + \nabla \cdot (\rho \mathbf{v}_i) = 0 \quad (1)$$

$$\rho \frac{d\mathbf{v}_i}{dt} = \nabla \cdot \boldsymbol{\tau}_{ij} + \rho g_i \quad (2)$$

$$\rho \frac{d(c_p \theta)}{dt} = \nabla(\kappa \nabla \theta) + Q_i \quad (3)$$

5 with the (constant) density ρ , the velocity vector $\mathbf{v}_i = (v_x, v_y, v_z) = (u, v, w)$, the gravitational acceleration $g_i = (0, 0, g)$, the stress tensor $\boldsymbol{\tau}_{ij}$, the (potential) temperature θ , the heat capacity c_p , the thermal conductivity κ , and the internal frictional heating Q_i . In the following we consider Cartesian coordinates, with the vertical coordinate z upwards and neglect acceleration. In case of an incompressible fluid with a constant density the continuity equation (conservation of mass) follows as

$$10 \nabla \cdot \mathbf{v}_i = \frac{\partial u}{\partial x} + \frac{\partial v}{\partial y} + \frac{\partial w}{\partial z} = 0. \quad (4)$$

The stress tensor is split into a deviatoric part $\boldsymbol{\tau}'_{ij}$ and an isotropic pressure p , which is defined as the trace of the stress tensor:

$$\begin{aligned} \boldsymbol{\tau}_{ij} &= \boldsymbol{\tau}'_{ij} - p \delta_{ij} \\ &= \boldsymbol{\tau}'_{ij} - \frac{1}{3}(\tau_{xx} + \tau_{yy} + \tau_{zz})\delta_{ij} \end{aligned} \quad (5)$$

where δ_{ij} symbolizes the Kronecker-delta.

GMDD

6, 3289–3347, 2013

Description of the multi-physics ice flow model RIMBAY

M. Thoma et al.

Title Page

Abstract

Introduction

Conclusions

References

Tables

Figures

⏪

⏩

◀

▶

Back

Close

Full Screen / Esc

Printer-friendly Version

Interactive Discussion



3.1 Equation of motion

The momentum equation can be written as

$$\begin{aligned} \frac{\partial \tau'_{xx}}{\partial x} + \frac{\partial \tau'_{xy}}{\partial y} + \frac{\partial \tau'_{xz}}{\partial z} - \frac{\partial p}{\partial x} &= 0 \\ \frac{\partial \tau'_{yx}}{\partial x} + \frac{\partial \tau'_{yy}}{\partial y} + \frac{\partial \tau'_{yz}}{\partial z} - \frac{\partial p}{\partial y} &= 0 \\ \frac{\partial \tau'_{zx}}{\partial x} + \frac{\partial \tau'_{zy}}{\partial y} + \frac{\partial \tau'_{zz}}{\partial z} - \frac{\partial p}{\partial z} &= \rho g \end{aligned} \quad (6)$$

According to Paterson (1994), the constitutive equation for polycrystalline ice links the deviatoric stresses to the strain rates

$$\begin{aligned} \tau'_{ij} &= 2\eta \dot{\epsilon}_{ij} = 2\eta \begin{pmatrix} \dot{\epsilon}_{xx} & \dot{\epsilon}_{xy} & \dot{\epsilon}_{xz} \\ \dot{\epsilon}_{yx} & \dot{\epsilon}_{yy} & \dot{\epsilon}_{yz} \\ \dot{\epsilon}_{zx} & \dot{\epsilon}_{zy} & \dot{\epsilon}_{zz} \end{pmatrix} \\ &= 2\eta \begin{pmatrix} \frac{\partial u}{\partial x} & \frac{1}{2} \left(\frac{\partial u}{\partial y} + \frac{\partial v}{\partial x} \right) & \frac{1}{2} \left(\frac{\partial u}{\partial z} + \frac{\partial w}{\partial x} \right) \\ \frac{1}{2} \left(\frac{\partial u}{\partial y} + \frac{\partial v}{\partial x} \right) & \frac{\partial v}{\partial y} & \frac{1}{2} \left(\frac{\partial v}{\partial z} + \frac{\partial w}{\partial y} \right) \\ \frac{1}{2} \left(\frac{\partial u}{\partial z} + \frac{\partial w}{\partial x} \right) & \frac{1}{2} \left(\frac{\partial v}{\partial z} + \frac{\partial w}{\partial y} \right) & \frac{\partial w}{\partial z} \end{pmatrix} \end{aligned} \quad (7)$$

applying the effective viscosity η , which can be described by the Glen-type flow law (e.g., Cuffey and Paterson, 2010)

$$\begin{aligned} \dot{\epsilon} &= A(\hat{\theta})\tau^n, \quad \text{or} \quad \tau_{ij} = 2\eta \dot{\epsilon}_{ij} \quad \text{with} \\ \eta &:= \frac{1}{2} A(\hat{\theta})^{-\frac{1}{n}} \dot{\epsilon}^{\frac{(1-n)}{n}} \end{aligned} \quad (8)$$

with $n = 3$, the pressure-corrected ice temperature $\hat{\theta} = \theta + \alpha p$, with a constant $\alpha = 9.8 \times 10^{-4} \text{ KPa}^{-1}$ or $8.7 \times 10^{-4} \text{ Km}^{-1}$ (Greve and Blatter, 2009), and the effective strain rate (valid for incompressibility as $\dot{\epsilon}_{xx}^2 + \dot{\epsilon}_{yy}^2 + \dot{\epsilon}_{zz}^2 = 0$ follows from Eq. 4)

$$\dot{\epsilon} = \sqrt{\dot{\epsilon}_{xx}^2 + \dot{\epsilon}_{yy}^2 + \dot{\epsilon}_{xx}\dot{\epsilon}_{yy} + \dot{\epsilon}_{xy}^2 + \dot{\epsilon}_{xz}^2 + \dot{\epsilon}_{yz}^2} \quad (9)$$

- 5 The temperature dependent *rate factor* $A(\hat{\theta})$ is parametrised according to the Arrhenius relationship after Hooke (1981) or Paterson and Budd (1982). Combining Eqs. (6) and (7) we get the so-called *Full Stokes* (FS) equations for ice modelling:

$$\begin{aligned} \frac{\partial}{\partial x} \left(2\eta \frac{\partial u}{\partial x} \right) + \frac{\partial}{\partial y} \left(\eta \frac{\partial u}{\partial y} + \eta \frac{\partial v}{\partial x} \right) + \frac{\partial}{\partial z} \left(\eta \frac{\partial u}{\partial z} + \eta \frac{\partial w}{\partial x} \right) - \frac{\partial p}{\partial x} &= 0 \\ \frac{\partial}{\partial x} \left(\eta \frac{\partial u}{\partial y} + \eta \frac{\partial v}{\partial x} \right) + \frac{\partial}{\partial y} \left(2\eta \frac{\partial v}{\partial y} \right) + \frac{\partial}{\partial z} \left(\eta \frac{\partial v}{\partial z} + \eta \frac{\partial w}{\partial y} \right) - \frac{\partial p}{\partial y} &= 0 \\ \frac{\partial}{\partial x} \left(\eta \frac{\partial u}{\partial z} + \eta \frac{\partial w}{\partial x} \right) + \frac{\partial}{\partial y} \left(\eta \frac{\partial v}{\partial z} + \eta \frac{\partial w}{\partial y} \right) + \frac{\partial}{\partial z} \left(2\eta \frac{\partial w}{\partial z} \right) - \frac{\partial p}{\partial z} &= \rho g \end{aligned} \quad (10)$$

Rearranging Eq. (5) leads to

$$\begin{aligned} p &= -\tau'_{xx} - \tau'_{yy} - \tau_{zz} \\ &= -2\eta \left(\frac{\partial u}{\partial x} + \frac{\partial v}{\partial y} \right) - \tau_{zz} \end{aligned} \quad (11)$$

with an expression for the vertical normal stress τ_{zz} obtained by vertically integrating the third equation of Eq. (6) from the surface S to the height z (Van der Veen and Whillans, 1989; Pattyn, 2008):

$$\tau_{zz} = -\rho g (S - z) + \underbrace{\frac{\partial}{\partial x} \int_z^S \tau'_{xz} dz' + \frac{\partial}{\partial y} \int_z^S \tau'_{yz} dz'}_{R_{zz}} \quad (12)$$

Here, the first term in Eq. (12) describes the hydrostatic part and R_{zz} the resistive part, sometimes also referred to as *vertical resistive longitudinal stress*.

Depending on the scientific issue, several approximations of Eq. (10) might be reasonable, which are described in the following subsection.

5 3.2 Higher-order approximation

The *Higher Order Model* (HOM) approximation of Pattyn (2003) applies the hydrostatic approximation, by neglecting the resistive stress R_{zz} in the Eqs. (10)–(12) for the vertical velocity and the vertical normal stress. These are only relevant (but still almost two orders of magnitude below the other normal stress and shear stress components, Pattyn, 2000) where the ice flow regime changes, as in the vicinity of ice margins or ice divides. Additionally, ignoring the horizontal derivatives of the vertical velocity in Eq. (10), leads to

$$\begin{aligned} \frac{\partial}{\partial x} \left(2\eta \frac{\partial u}{\partial x} \right) + \frac{\partial}{\partial y} \left(\eta \frac{\partial u}{\partial y} + \eta \frac{\partial v}{\partial x} \right) + \frac{\partial}{\partial z} \left(\eta \frac{\partial u}{\partial z} \right) - \frac{\partial \rho}{\partial x} &= 0 \\ \frac{\partial}{\partial x} \left(\eta \frac{\partial u}{\partial y} + \eta \frac{\partial v}{\partial x} \right) + \frac{\partial}{\partial y} \left(2\eta \frac{\partial v}{\partial y} \right) + \frac{\partial}{\partial z} \left(\eta \frac{\partial v}{\partial z} \right) - \frac{\partial \rho}{\partial y} &= 0 \\ \frac{\partial}{\partial z} \left(2\eta \frac{\partial w}{\partial z} \right) - \frac{\partial \rho}{\partial z} &= \rho g \end{aligned} \quad (13)$$

Applying Eqs. (11) and (12) we obtain

$$\begin{aligned} \frac{\partial}{\partial x} \left[2\eta \left(2 \frac{\partial u}{\partial x} + \frac{\partial v}{\partial y} \right) \right] + \frac{\partial}{\partial y} \left[\eta \left(\frac{\partial u}{\partial y} + \frac{\partial v}{\partial x} \right) \right] + \frac{\partial}{\partial z} \left(\eta \frac{\partial u}{\partial z} \right) &= \rho g \frac{\partial S}{\partial x} \\ \frac{\partial}{\partial y} \left[2\eta \left(2 \frac{\partial v}{\partial y} + \frac{\partial u}{\partial x} \right) \right] + \frac{\partial}{\partial x} \left[\eta \left(\frac{\partial u}{\partial y} + \frac{\partial v}{\partial x} \right) \right] + \frac{\partial}{\partial z} \left(\eta \frac{\partial v}{\partial z} \right) &= \rho g \frac{\partial S}{\partial y} \end{aligned} \quad (14)$$

for the horizontal velocities. The vertical velocity at depth z can be derived by integrating the continuity equation Eq. (4) from the base B vertically:

$$w(z) = w(B) - \int_B^z \left(\frac{\partial u}{\partial x} + \frac{\partial v}{\partial y} \right) dz' \quad (15)$$

3.3 Shallow-shelf or shelfy-stream approximation

5 A second common approximation is the *Shallow Shelf Approximation* or *Shelfy Stream Approximation* (SSA). This assumes that the horizontal velocity is depth-independent ($\frac{\partial u}{\partial z} = \frac{\partial v}{\partial z} = 0$), which is the case for ice shelf regions and fast flowing ice streams decoupled from the ground. Integrating Eq. (14) through the ice from the base B to the surface S , and defining U and V as the vertically integrated velocities leads to (e.g. 10 MacAyeal, 1989; Pattyn, 2010)

$$\begin{aligned} \frac{\partial}{\partial x} \left[2H\eta \left(2\frac{\partial U}{\partial x} + \frac{\partial V}{\partial y} \right) \right] + \frac{\partial}{\partial y} \left[H\eta \left(\frac{\partial U}{\partial y} + \frac{\partial V}{\partial x} \right) \right] - \tau_{bx} &= \rho g H \frac{\partial S}{\partial x} \\ \frac{\partial}{\partial y} \left[2H\eta \left(2\frac{\partial V}{\partial y} + \frac{\partial U}{\partial x} \right) \right] + \frac{\partial}{\partial x} \left[H\eta \left(\frac{\partial U}{\partial y} + \frac{\partial V}{\partial x} \right) \right] - \tau_{by} &= \rho g H \frac{\partial S}{\partial y} \end{aligned} \quad (16)$$

where the basal shear stress τ_{bi} retards the otherwise unhampered flow on bedrock till. It can be expressed in terms of the basal friction parameter β^2 and the horizontal velocity: $\tau_{bi} = \beta^2 V_j$. A thorough derivation of Eq. (16) can be found in Greve and Blatter 15 (2009). Both, the *Shelfy Stream Approximation* and the *Shallow Shelf Approximation* are expressed by Eq. (16). The only difference is, that for an ice shelf or above a subglacial lake β^2 is zero, while it might reach several thousand Pa s^{-1} for a slippery bedrock, which especially applies to basal lubricated areas. As a rule of thumb above dry bedrock a value of $\beta^2 = 25\,000 \text{ Pa yr m}^{-1}$ would correspond to a typical frictional 20 stress of about 100 kPa (Paterson, 1994) if a velocity of about 4 m yr^{-1} is assumed

(Thoma et al., 2012). Finally, because of the lacking vertical shear stresses Eq. (9) reduces to

$$\dot{\epsilon} = \sqrt{\dot{\epsilon}_{xx}^2 + \dot{\epsilon}_{yy}^2 + \dot{\epsilon}_{xx}\dot{\epsilon}_{yy} + \dot{\epsilon}_{xy}^2} \quad (17)$$

3.4 Shallow ice approximation

5 The most rigid approximation is the Shallow Ice Approximation (SIA), which is a reasonable simplification for large ice bodies, when the horizontal length scale is much larger than the vertical scale (ice thickness). Assuming that the horizontal derivation of the vertical velocity is much smaller than the vertical derivation of the horizontal velocity ($\frac{\partial w}{\partial x} \ll \frac{\partial u}{\partial z}$) and applying the hydrostatic approximation (which reduces the vertical momentum balance to the hydrostatic term) we derive

$$\begin{aligned} \frac{\partial}{\partial z} \left(\eta \frac{\partial u}{\partial z} \right) - \frac{\partial p}{\partial x} &= 0 \\ \frac{\partial}{\partial z} \left(\eta \frac{\partial v}{\partial z} \right) - \frac{\partial p}{\partial y} &= 0 \\ - \frac{\partial p}{\partial z} &= \rho g \end{aligned} \quad (18)$$

Basically, this approximation decouples the horizontal velocities, allowing local solutions for the velocity field, instead of much more complex and time-consuming implicit solver. The numerical resources of this SIA are so low (compared to any other approximations), that it is still widely used (and useful) for many applications.

3.5 Boundary conditions

Several boundary conditions have to be formulated to solve the different approximations of the equation of motion.

Description of the multi-physics ice flow model RIMBAY

M. Thoma et al.

Title Page	
Abstract	Introduction
Conclusions	References
Tables	Figures
◀	▶
◀	▶
Back	Close
Full Screen / Esc	
Printer-friendly Version	
Interactive Discussion	

1. We apply a stress-free surface boundary condition

$$\tau_{ij}(S) \cdot n_s = 0 \tag{19}$$

with the normal vector n_s orthogonal to the surface.

2. For the horizontal velocities at the ice base, we apply either

- a no-slip condition ($u_B = v_B = 0$),
- a Weertman-type sliding law (e.g. Paterson, 1994; Cuffey and Paterson, 2010), linking the sliding velocity with the basal shear stress

$$\begin{aligned} \tau_{bi} &= \beta^2 v_i(B) = C^{\frac{1}{m}} |v_i(B)|^{m-1} v_i(B) \quad \text{or} \\ v_i(B) &= \frac{1}{\beta^2} \tau_{bi} = C^{-\frac{1}{m}} |\tau_{bi}|^{\frac{1}{(m-1)}} \tau_{bi} \end{aligned} \tag{20}$$

with $i = (x, y)$, the basal friction coefficient C , and the basal friction exponent m .

The basal drag is defined as the sum of all basal resistive forces (Van der Veen and Whillans, 1989; Pattyn, 2003)

$$\begin{aligned} \tau_{bx} &= \tau'_{xz} - (2\tau'_{xx} + \tau'_{yy}) \frac{\partial B}{\partial x} - \tau'_{xy} \frac{\partial B}{\partial y} \\ \tau_{by} &= \tau'_{yz} - (2\tau'_{yy} + \tau'_{xx}) \frac{\partial B}{\partial y} - \tau'_{xy} \frac{\partial B}{\partial x} \end{aligned} \tag{21}$$

with $\tau'_{ij} = \tau'_{ij}(B)$. In case of the (SIA) these equations simplify to

$$\tau_{bx} = -\rho g H \frac{\partial S}{\partial x}, \quad \tau_{by} = -\rho g H \frac{\partial S}{\partial y} \tag{22}$$

- or a stress free base when a substantial amount of water is present, like in the case of subglacial lakes and ice shelves; this implies $\beta^2 = 0$.



Description of the multi-physics ice flow model RIMBAY

M. Thoma et al.

Title Page

Abstract

Introduction

Conclusions

References

Tables

Figures

◀

▶

◀

▶

Back

Close

Full Screen / Esc

Printer-friendly Version

Interactive Discussion



3. For the vertical velocity at the base, we apply a kinematic boundary condition

$$w_B = \frac{\partial B}{\partial t} + u \frac{\partial B}{\partial x} + v \frac{\partial B}{\partial y} - \dot{m}_B \quad (23)$$

with the basal melt rate \dot{m}_B .

4. At lateral boundaries of the model domain, we apply either

- zero ice thickness ($H = 0$),
- Dirichlet boundary conditions with fixed velocities. The no-slip condition ($u = 0$), which would imply frozen ice at nunataks, is a special case of this.
- A Neumann free-slip boundary conditions $\nabla \mathbf{v}_i \cdot \mathbf{n}_i = 0$ at ice-nunatak edges, or
- a (dynamic) Neumann boundary conditions for an ice shelf–ocean-interface (e.g. Greve and Blatter, 2009; Joughin et al., 2009; Pattyn, 2010),

$$2\mu H \left(2 \frac{\partial U}{\partial x} + \frac{\partial V}{\partial y} \right) n_x + \mu H \left(\frac{\partial U}{\partial y} + \frac{\partial V}{\partial x} \right) n_y = \frac{\rho g H S n_x}{2} \quad (24)$$

$$2\mu H \left(2 \frac{\partial V}{\partial y} + \frac{\partial U}{\partial x} \right) n_y + \mu H \left(\frac{\partial V}{\partial x} + \frac{\partial U}{\partial y} \right) n_x = \frac{\rho g H S n_y}{2}$$

with the outward-pointing unit vector (n_x, n_y) , which is perpendicular to the (vertical) ice shelf front.

- or periodic boundary conditions.

As usual for ice sheet/shelf modelling, these equations are converted in terrain following σ -coordinates by applying

$$\sigma = \frac{S - z}{H}, \quad (25)$$

with the ice thickness H and the surface height S . This coordinate transformation leads to additional metric terms in the equations, which are described in detail in Pattyn (2003) or Greve and Blatter (2009). The advantage is, that the vertical coordinate ranges from $\sigma = 0$ at the surface to $\sigma = 1$ at the ice base, independent of the local ice thickness and the bedrock elevation.

3.6 Temperature calculation

Assuming a constant heat capacity c_p and thermal conductivity k , the temperature evolution (Eq. 3) can be divided into an advective, a diffusive and a source term

$$\rho c_p \left(\frac{\partial \theta}{\partial t} + \underbrace{\mathbf{v}_i \nabla \theta}_{\text{Advection}} \right) = \underbrace{k \nabla^2 \theta}_{\text{Diffusion}} + \underbrace{Q_i}_{\text{Internal Sources}} \quad (26)$$

Neglecting horizontal diffusion and assuming, that the internal heat source results mainly from the ice deformation (Paterson, 1994) we obtain with the effective deviatoric stress τ' and $Q_i = 2\dot{\epsilon}\tau' = 4\eta\dot{\epsilon}^2$

$$\frac{\partial \theta}{\partial t} = \frac{k}{\rho c_p} \frac{\partial^2 \theta}{\partial z^2} - u \frac{\partial \theta}{\partial x} - v \frac{\partial \theta}{\partial y} - w \frac{\partial \theta}{\partial z} + 4\eta\dot{\epsilon}^2 \quad (27)$$

The boundary conditions applied to solve this thermodynamic equation are

- the mean air temperature at the surface of the ice body,
- a Dirichlet boundary condition according to the pressure melting point of ice (e.g., Paterson, 1994) $\theta = -8.7 \times 10^{-4} \text{ K m}^{-1} \cdot H$ at the ice base when the ice is floating (like above subglacial lakes and for ice shelves), and
- a Neumann boundary condition at the base B for grounded ice

$$\frac{\partial \theta_B}{\partial z} = - \frac{G + \tau'_B |\mathbf{v}_i(B)|}{k} \quad (28)$$

Title Page

Abstract

Introduction

Conclusions

References

Tables

Figures

◀

▶

◀

▶

Back

Close

Full Screen / Esc

Printer-friendly Version

Interactive Discussion



with the basal stress $\tau'_B = \sqrt{t_{bx}^2 + t_{by}^2}$ and the geothermal heat flux G .

3.7 Ice sheet evolution

Integration of Eq. (1) from the base B to the surface S leads to an equation for the ice evolution. Defining the ice thickness $H = S - B$, accounting for melting or accumulation at the surface and/or base and assuming a constant ice density ρ we get

$$\frac{\partial}{\partial t} \int_B^S \rho dz + \nabla \cdot \int_B^S (\rho \mathbf{v}_i) dz = \dot{m} \quad (29)$$

$$\frac{\partial H}{\partial t} = - \left(\frac{\partial UH}{\partial x} + \frac{\partial VH}{\partial y} \right) + \dot{m} \quad (30)$$

with the mass balance defined as

$$\dot{m} = \underbrace{\dot{m}_{ac}}_{\text{Accumulation}} - \underbrace{\dot{m}_{ab}}_{\text{Ablation}} - \underbrace{\dot{m}_B}_{\text{Basal melting}} \quad (31)$$

Basal freezing can be implemented by negative basal melting.

4 Numerical model

4.1 Linear and non-linear solvers

The coupled pair of linear equations for the horizontal velocity field for the Full Stokes (FS), Higher Order Model (HOM), and (SSA) Eqs. (10), (14), and (16) depend on the strain-rate dependent viscosity Eq. (8), resulting in a non-linear problem. However, this problem can be solved iteratively as indicated by Fig. 2.

According to Pattyn (2003), it is sufficient to solve the system of linear equations for u and v successively, instead of solving both equations at once. This two-step approach results in less memory consumption, faster convergence and an equal stability solution. In general, we iteratively solve

$$5 \quad \mathbf{A}_{nm}(x_{ij}^l) \cdot x_m^{l+1} = b_n(x_{ij}^l) \quad (32)$$

where l is the iteration, \mathbf{A}_{nm} contains the coefficients of the left-hand side of the relevant equation to solve, while b_n is the forcing term on the right-hand side of the equation. The placeholder x_m symbolizes the horizontal velocities u_{ij} or v_{ij} (Eqs. 10, 14, or 16), the potential temperature θ_{ij} (Eq. 27), or the ice thickness H_{ij} (Eq. 30), respectively. The indices n and m symbolize the consecutively numbered grid nodes from ($j = 1, i = 1$) to ($j = X_{\max}, i = Y_{\max}$)¹.

Two methods to solve the linear system of Eq. (32) are available within RIMBAY: first, the fast and efficient biconjugate gradient method with a Jacobian preconditioner (*linbcg*) from Press et al. (2007), second the *Library of Iterative Solvers* (LIS) from Nishida (2010). The Library of Iterative Solvers (LIS) provides a bunch of preconditioners and solvers, including the recommendable *Generalized Minimal RESidual* (gmres) method, which can also be applied to solve non-symmetric matrices. For both methods the effective *compressed row storage* (CRS) sparse matrix method is used as a default to store the elements of the matrix \mathbf{A}_{nm} . However, for the LIS, the *modified sparse row* (MSR) format is implemented, too. Comparisons with respect to the calculated velocities have shown

- the differences for the two storage formats (CRS vs. MSR) are negligible,
- the differences between the *linbcg* solver from Press et al. (2007) and the very same preconditioner/solver combination from the *Library of Iterative Solvers* are

¹Note, that for historical reasons (originating from Pattyn, 2003, 2008) the order of i and j is swapped within RIMBAY, compared with the intuitive usage.

Description of the multi-physics ice flow model RIMBAY

M. Thoma et al.

Title Page	
Abstract	Introduction
Conclusions	References
Tables	Figures
◀	▶
◀	▶
Back	Close
Full Screen / Esc	
Printer-friendly Version	
Interactive Discussion	



negligible, but the solver of Press et al. (2007) needs less computational resources.

- *if* specific preconditioner–solver combination converge, the difference between different combinations are negligible.

5 Summarised, *if* a solution of the linear system can be computed with a reasonable accuracy, the results can be trusted. In general, we suggest to start with the faster *linbcg* algorithm (from Press et al., 2007) and to switch to the *gmres* solver with a Jacobian or ILU (Incomplete LU decomposition) preconditioner if it should fail.

10 When solving the linearized equations for the horizontal velocity, the viscosity η might vary over a few orders of magnitude, which requires a sophisticated convergence scheme. Hence, a simple Picard iteration might fail. Therefore, Pattyn (2003) extended this scheme by the *unstable manifold correction* (UMC), introduced by Hindmarsh and Payne (1996), which results in a proper convergence of the solution. In RIMBAY the UMC is applied in the SSA, HOM, and FS solvers.

15 4.2 Discretisation

When equations are discretised, it is important to realize where exactly the individual variables are located. This is quite simply defined for the unstaggered Arakawa A-Grid (e.g., Arakawa and Lamb, 1977; Purser and Leslie, 1988) where all variables are located in the very same grid position. However, sometimes a different approach has numerical advantages. Besides the traditional (unstaggered) A-Grid, the staggered
20 Arakawa C-Grid is optionally available in RIMBAY for the SIA- and SSA-solvers. On the Arakawa C-Grid, the horizontal velocities are defined inbetween the thickness (and viscosity) nodes as illustrated in Fig. 3.

GMDD

6, 3289–3347, 2013

Description of the multi-physics ice flow model RIMBAY

M. Thoma et al.

Title Page

Abstract

Introduction

Conclusions

References

Tables

Figures

⏪

⏩

◀

▶

Back

Close

Full Screen / Esc

Printer-friendly Version

Interactive Discussion



4.3 Ice sheet evolution

As an example, we formulate the implemented discretisation of the ice sheet evolution (Eq. 30) explicitly for the two different grids. Additionally, the detailed discretisation on the C-grid of the SSA equation of motion (Eq. 16) is given in Appendix B.

4.3.1 C-Grid

For the C-Grid, where the velocities are defined inbetween thickness nodes, the equation of the ice sheet evolution (Eq. 30) can be written as an implicit first order finite difference equation as

$$\begin{aligned}
 H_{i,j}^{t+1} + \frac{\Delta t \left[U_{i,j}(H_{i,j+1}^{t+1} + H_{i,j}^{t+1}) - U_{i,j-1}(H_{i,j}^{t+1} + H_{i,j-1}^{t+1}) \right]}{2\Delta x} \\
 + \frac{\Delta t \left[V_{i,j}(H_{i+1,j}^{t+1} + H_{i,j}^{t+1}) - V_{i-1,j}(H_{i,j}^{t+1} + H_{i-1,j}^{t+1}) \right]}{2\Delta y} \\
 = H_{i,j}^t + \dot{m}\Delta t
 \end{aligned} \tag{33}$$

Rearranging Eq. (33) with respect to the five discrete H^{t+1} -values, located and numbered as indicated by Fig. 4, results in the following coefficients for the sparse matrix \mathbf{A}_{nm} of the linear solver:

$$C_{n1} = -\frac{\Delta t}{2\Delta y} V_{i-1,j}$$

$$C_{n2} = -\frac{\Delta t}{2\Delta x} U_{i,j-1}$$

$$C_{n3} = 1 + \frac{\Delta t}{2} \left(\frac{U_{i,j} - U_{i,j-1}}{\Delta x} + \frac{V_{i,j} - V_{i-1,j}}{\Delta y} \right)$$

$$\begin{aligned}
C_{n4} &= + \frac{\Delta t}{2\Delta x} U_{i,j} \\
C_{n5} &= + \frac{\Delta t}{2\Delta y} V_{i,j} \\
b_n &= H_{i,j}^t + \dot{m}_{i,j} \Delta t
\end{aligned} \tag{34}$$

- 5 These coefficients represent the non-zero elements of each single row n for each ij -element of the matrix \mathbf{A}_{nm} , with C_{n3} indicating the central node at (i,j) and b_n indicates the forcing term on the right-hand-side.

4.3.2 Boundary conditions for the C-Grid

10 The coefficients derived in the last subsection are valid for the interior of the ice. Boundary conditions have to be formulated at the edges of the ice sheet. *Open boundaries* for grid cells adjacent to ocean or ice-free land are simply implicitly implemented by assuming $H = 0$ at the respective grid cell.

15 If the ice adjoins a nunatak or a lateral end of the model domain, *closed boundary* conditions are applied. We define these by setting the velocity (and thus the flux) of ice over the edge of the specific grid cell, to zero. For example, closed boundaries at the eastern ($U_{i,j} = 0$) and southern ($V_{i-1,j} = 0$) edge would result in $C_{n1} = C_{n4} = 0$ and $C_{n3} = 1 + \frac{\Delta t}{2} \left(\frac{V_{i,j}}{\Delta y} - \frac{U_{i,j-1}}{\Delta x} \right)$ in Eq. (34).

4.3.3 A-Grid

20 For the the A-Grid a pure advective scheme to solve Eq. (30) would be numerically problematic. Hence, we decompose the equation into a weighted advective and diffusive part by applying the identity $(\nabla H + \nabla B)(\nabla S)^{-1} = 1$, derived from a simple gradient formulation of $S = H + B$ (surface elevation S equals ice thickness H plus ice bottom

Description of the multi-physics ice flow model RIMBAY

M. Thoma et al.

Title Page

Abstract

Introduction

Conclusions

References

Tables

Figures

⏪

⏩

◀

▶

Back

Close

Full Screen / Esc

Printer-friendly Version

Interactive Discussion



B):

$$\frac{\partial H}{\partial t} + f_{\text{ad}} \nabla \cdot \left[V_i H (\nabla S)^{-1} (\nabla H + \nabla B) \right] + (1 - f_{\text{ad}}) \nabla \cdot (V_i H) = \dot{m} \quad (35)$$

5 with $f_{\text{ad}} = 1$ for pure diffusion and $f_{\text{ad}} = 0$ in case of pure advection. With the definition of the non-linear (because it depends on the solution H) diffusion vector $D_i := (D_x, D_y) = -V_i H (\nabla S)^{-1}$ we derive

$$\frac{\partial H}{\partial t} - f_{\text{ad}} \nabla \cdot (D_i \nabla H) + (1 - f_{\text{ad}}) \nabla \cdot (V_i H) = f_{\text{ad}} \nabla \cdot (D_i \nabla B) + \dot{m} \quad (36)$$

The finite difference formulation of Eq. (36) as well as the coefficients C_{nm} for the sparse linear matrix for the interior and the boundary conditions are given in the Appendix A. In general, it would be appropriate to apply the diffusive equation (with $f_{\text{ad}} = 1$), because a *Lax-Method* has to be used to numerically stabilise the advective part of Eq. 36 (see Appendix A). Unfortunately, this adds numerical dissipation (numerical diffusion) and results in a time-step dependence of the solution. However, if the ice body contains ice shelves and/or ice divides with flat areas, the reciprocal value of $(\nabla S)^{-1}$ becomes very large and counteracts the stabilising effect of the otherwise stable diffusive implementation. Despite this problem of exchanging stability towards convergence (with respect to decreasing timesteps) this approach has discussed in some applications (e.g., Pattyn et al., 2006; Docquier et al., 2011).

As an alternative to overcome the restrictions involved with the numerical representation of Eq. (35), we implemented a mass conserving (timestep independent) upwind scheme, based on Eq. (33). Averaging the horizontal velocities from their central (A-grid) location towards the grid-cell edges according to $U_{i,j}^c = (U_{i,j} + U_{i,j+1})$ and

GMDD

6, 3289–3347, 2013

Description of the multi-physics ice flow model RIMBAY

M. Thoma et al.

Title Page

Abstract

Introduction

Conclusions

References

Tables

Figures

◀

▶

◀

▶

Back

Close

Full Screen / Esc

Printer-friendly Version

Interactive Discussion



$V_{i,j}^c = (V_{i,j} + V_{i+1,j})$ leads to

$$\begin{aligned}
 H_{i,j}^{t+1} &+ \frac{\Delta t}{2\Delta x} \left[(U_{i,j}^c + |U_{i,j}^c|) H_{i,j}^{t+1} + (U_{i,j}^c - |U_{i,j}^c|) H_{i,j+1}^{t+1} \right. \\
 &- (U_{i,j-1}^c + |U_{i,j-1}^c|) H_{i,j-1}^{t+1} - (U_{i,j-1}^c - |U_{i,j-1}^c|) H_{i,j}^{t+1} \left. \right] \\
 &+ \frac{\Delta t}{2\Delta y} \left[(V_{i,j}^c + |V_{i,j}^c|) H_{i,j}^{t+1} + (V_{i,j}^c - |V_{i,j}^c|) H_{i+1,j}^{t+1} \right. \\
 &- (V_{i-1,j}^c + |V_{i-1,j}^c|) H_{i,j}^{t+1} - (V_{i-1,j}^c - |V_{i-1,j}^c|) H_{i-1,j}^{t+1} \left. \right] \\
 &= H_{i,j}^t + \dot{m} \Delta t
 \end{aligned} \tag{37}$$

and the following coefficients for the sparse matrix \mathbf{A}_{nm} :

$$\begin{aligned}
 C_{n1} &= -\frac{\Delta t}{2\Delta y} (V_{i-1,j}^c + |V_{i-1,j}^c|) \\
 C_{n2} &= -\frac{\Delta t}{2\Delta x} (U_{i,j-1}^c + |U_{i,j-1}^c|) \\
 C_{n3} &= 1 + \frac{\Delta t}{2} \left(\frac{(U_{i,j}^c + |U_{i,j}^c|) - (U_{i,j-1}^c - |U_{i,j-1}^c|)}{\Delta x} + \frac{(V_{i,j}^c + |V_{i,j}^c|) - (V_{i-1,j}^c - |V_{i-1,j}^c|)}{\Delta y} \right) \\
 C_{n4} &= +\frac{\Delta t}{2\Delta x} (U_{i,j}^c - |U_{i,j}^c|) \\
 C_{n5} &= +\frac{\Delta t}{2\Delta y} (V_{i,j}^c - |V_{i,j}^c|) \\
 b_n &= H_{i,j}^t + \dot{m}_{i,j} \Delta t
 \end{aligned} \tag{38}$$

5 4.4 Ice sheet–ice shelf coupling and grounding line flux

The solution of a coupled ice sheet–ice shelf system is numerically complicated, if not solved with a high-resolution FS approach. According to Pattyn et al. (2013) a hori-

Title Page

Abstract

Introduction

Conclusions

References

Tables

Figures

◀

▶

◀

▶

Back

Close

Full Screen / Esc

Printer-friendly Version

Interactive Discussion



zontal resolution of less than 0.5 km is necessary to capture the grounding line (GRL) migration accurately. This however, is computationally costly and inefficient, especially for the shelf, which demands only reduced physics (comp. Eq. 18). Either a finite element discretisation (as in the Elmer/Ice model, e.g. Zwinger et al., 2007) or adaptive grids (Gladstone et al., 2010) with varying grid sizes are necessary to implement the FS approach in a reasonable way. For coarse resolution finite difference models (with a grid sizes beyond one kilometer), Pollard and DeConto (2009) and Pollard and DeConto (2012) suggested a heuristic approach, based on the semi-analytical grounding line flux solution, derived by Schoof (2007)

$$Q_i^S = \left(\frac{A(\rho g)^{n+1} (1 - \rho/\rho_{\text{Ocean}})^n}{4^n C} \right)^{\frac{1}{m+1}} \left(\frac{\tau'_{ii}}{\tau_f} \right)^{\frac{n}{m+1}} h_g^{\frac{m+n+3}{m+1}} \quad (39)$$

with the direction i being either x or y , the longitudinal stress τ'_{ii} just downstream of the grounding line, and the unbuttressed stress $\tau_f = 0.5 \rho g h_g (1 - \rho/\rho_{\text{Ocean}})$. The grounding line flux Q_i^S is estimated from the ice thickness h_g at the interpolated sub-grid grounding line position. Before the ice evolution Eq. (29) is solved, the Schoof-flux (estimated on a sub-grid scale) constrains the flux across the grounding line by correcting the previous estimated velocity, located on a discrete grid-node according to

$$\begin{aligned} \mathbf{v}_i &= \frac{Q_i^S}{H} & \text{A-Grid,} \\ \mathbf{v}_i &= \frac{2Q_i^S}{H + H_{\text{float}}} & \text{C-Grid.} \end{aligned} \quad (40)$$

With the ice thickness H at the last grounded node (the model's grounding line) and H_{float} the ice thickness at the first floating node downstream. The distinction depends on the relation between the analytical Schoof-flux Q_i^S and the modelled flux through the last gridded node $Q_i^M = V_i H$ (or $Q_i^M = V_i \cdot 0.5(H + H_{\text{float}})$ on a C-Grid): if $Q_i^S \geq Q_i^M$ then

GMDD

6, 3289–3347, 2013

Description of the multi-physics ice flow model RIMBAY

M. Thoma et al.

Title Page

Abstract

Introduction

Conclusions

References

Tables

Figures

◀

▶

◀

▶

Back

Close

Full Screen / Esc

Printer-friendly Version

Interactive Discussion



more ice is transported into the ice shelf and the grounding line retreats or stays constant, the velocity at the grounding line is corrected according to Eq. (40). If $Q_i^S < Q_i^M$ than less ice is transported into the ice shelf and more ice is kept in the ice sheet, the grounding line advances and the velocity of the first floating node is corrected according to Eq. (40). A detailed description of this method, which we refer to as *schoofism* is given in Docquier et al. (2011), Pollard and DeConto (2012), and Pattyn et al. (2012). To avoid unrealistic velocity steps, we additionally apply a conservative 2-D-gaussian filter to the grounding line nodes to smooth the resulting velocity field.

5 Implementation

5.1 General information

The RIMBAY-code is mainly written in C++ and has about 30 000 (mostly) well documented lines. For historical reasons the code is not completely object oriented yet, but the level of classification is large and the number of global variables (which should be avoided as much as possible in any code) is close to zero. A reasonable degree of code separation into several C++-classes, allows an easy maintenance of the code. Well-defined interfaces (public-methods of the C++-classes) enable an easy extension of the code for upcoming developments in ice modelling and/or further reaching applications (see Sect. 7).

The *GNU build system*² (also known as the *autotools*) is a suite of programming tools designed to assist in making source-code packages portable to many Unix-like systems. It handles *Makefiles* and attends dependencies between different source (and header) files automatically. Thanks to the *GNU build system* RIMBAY has been compiled and tested successfully on several different Unix-platforms without any code adjustments. To distribute, develop, and maintain RIMBAY we use the distributed revision

²http://en.wikipedia.org/wiki/GNU_build_system

Description of the multi-physics ice flow model RIMBAY

M. Thoma et al.

Title Page

Abstract

Introduction

Conclusions

References

Tables

Figures

⏪

⏩

◀

▶

Back

Close

Full Screen / Esc

Printer-friendly Version

Interactive Discussion



control system *monotone*³, which keeps track of any changes within the code and provides a sophisticated automatic merging of development branches.

One of the main programming paradigms for RIMBAY is that the very same (compiled) code has to run every single (previous successfully tested) scenario without any code editing and/or recompiling. To achieve this, RIMBAY is started with command-line arguments and loads the specific scenario from parameter files and (if requested) optionally from a netcdf-file, too. The well established netcdf-output format of RIMBAY ensures that the computed results can subsequently post-processed with the desired software packages, if the supplied GMT-bash scripts (Wessel and Smith, 1998) (included in the RIMBAY-monotone database) should not be sufficient.

The RIMBAY code comes with a test-suit containing nearly 50 different scenarios. These small and fast-running scenarios are designed to ensure that future model developments do not interfere with previous results.

5.2 Solver coupling

The coupling of SIA and SSA at the grounding line, for instance, is realised by using the estimated velocities from the SIA solver as a Dirichlet boundary condition for the SSA solver. This transition can be located either at the last grounded node (the numerical GRL) or several grid-nodes inside the ice sheet. In the latter case a *transition zone* (or *grounding zone*) is defined by a region where the solutions of the SIA- and the SSA-solver are interpolated.

If the HOM/FS should not be applied to the whole model domain (which might be reasonable to save computational time), one or more *region(s) of interest* can be defined. In that case, the resource-consuming HOM/FS-solver is limited to these regions only, while the faster SIA and SSA-solvers are applied elsewhere and provide the Dirichlet boundary conditions for the HOM/FS-solver (see example in Sect. 6.4).

³<http://www.monotone.ca/>

GMDD

6, 3289–3347, 2013

Description of the multi-physics ice flow model RIMBAY

M. Thoma et al.

Title Page

Abstract

Introduction

Conclusions

References

Tables

Figures

⏪

⏩

◀

▶

Back

Close

Full Screen / Esc

Printer-friendly Version

Interactive Discussion



6 Validation

The implementation of the different mathematical models (SIA, SSA, HOM, and FS) to calculate the horizontal velocity field are validated separately in this subsection. Additionally we show, that the solver for the ice sheet evolution and the solver-coupling produces reasonable results. The temperature evolution and thermomechanical coupling is not reconsidered here. Although the solvers have been revised, their results are identical to those published by Pattyn (2003) and Thoma et al. (2012).

6.1 SIA-solver

The A-Grid implementation of the SIA within RIMBAY is mainly identical to those of Pattyn (2003) and has already been validated successfully against the *moving-margin Eis-mint* benchmark described in Huybrechts and Payne (1996) within Pattyn (2003). Here, we compare the estimated ice thicknesses, derived with the A-Grid (Type-II according to Huybrechts and Payne, 1996) and the C-Grid RIMBAY implementation for the *fixed- and moving margin* benchmark experiments, with results published by Huybrechts and Payne (1996) and Bueler et al. (2005). Figure 5 shows that the A-Grid implementation produces results very close to the reference, while the C-Grid implementation results in a 0.38 % larger ice thickness. Considering the very different discretisations (compare Eqs. 33 and A2) of the ice evolution equation, this is acceptable.

6.2 SSA-solver

The A- and the C-Grid implementations of the SSA are compared with a diagnostic tabular iceberg experiment of Jansen et al. (2005). In this experiment, the horizontal velocity field of a rectangular iceberg with a constant thickness of 250 m and an isothermal temperature of -20°C is calculated. The viscosity is calculated according to Eq. (8) with $n = 3$ and a temperature dependent rate factor given by the Arrhenius relationship after Paterson and Budd (1982). Our horizontal velocities are calculated on

GMDD

6, 3289–3347, 2013

Description of the multi-physics ice flow model RIMBAY

M. Thoma et al.

Title Page

Abstract

Introduction

Conclusions

References

Tables

Figures

◀

▶

◀

▶

Back

Close

Full Screen / Esc

Printer-friendly Version

Interactive Discussion



a 1 km grid and are in close agreement with those presented by Jansen et al. (2005) (Fig. 6a). Additionally, we rotate the iceberg, to demonstrate the independence of the model results from the iceberg's orientation within the rectangular grid (Fig. 6b–e). This test is essential for the modelling of evolving ice sheet fronts, which are rarely aligned with the grid orientation in real geometries.

A much more complex proof-of-concept is shown in Fig. 7. This artificially constructed geometry with a grid resolution of 2 km features

- a non-constant ice thickness,
- two discontinuous areas, which are solved simultaneously by the numerical solver,
- a quite complex shaped ice-water front with corners, tongues, and an inlet at $x \approx 200$ km.
- The brown areas in Fig. 7 symbolises nunataks, where special boundary conditions are applied: in the south ($y = 0$), a no-slip boundary results in stagnation at the ice-nunatak interface, while at the northern edge ($y = 220$ km) of the right iceberg a free-slip boundary condition is applied.
- Additionally, a small nunatak (with an area of $10 \text{ km} \times 5 \text{ km} = 50 \text{ km}^2$) located within the left iceberg with free-slip boundary conditions is added.

The modelled velocity pattern is consistent with the expectations, which are

- higher velocities at higher ice fronts,
- zero velocities at no-slip boundaries, and
- a reduced, orthogonally orientated velocity field at free-slip boundaries.

The difference between the A-Grid and the C-Grid (not shown) are negligible. Therefore, we conclude that the SSA-solver implementations produces reasonable and robust results, even for complex geometries.

Description of the multi-physics ice flow model RIMBAY

M. Thoma et al.

Title Page

Abstract

Introduction

Conclusions

References

Tables

Figures



Back

Close

Full Screen / Esc

Printer-friendly Version

Interactive Discussion



6.3 SIA–SSA-solver coupling and GRL-migration

Recently, RIMBAY participated in the *Marine Ice Sheet Model Intercomparison Project* (MISMIP)-3-D, which investigates the grounding line response to external forcings (Pattyn et al., 2013). For this experiment a coupled SIA–SSA solver with a transition zone of 150 km and *schoofism*, according to the method described in Sect. 4.4 was applied. We performed these scenarios with a comparable coarse resolution of 5 and 10 km, because our main focus was on the applicability of these approximations with respect to large-scale modelling, possibly coupled with an atmosphere and ocean model un an Earth-System model approach. In order to overcome the problem of capturing grounding line migration in coarse resolutions, we apply the heuristic rule described in Sect. 4.4. In consideration of the approximations and the low horizontal resolution, RIMBAY was able to keep up with the other 16 numerical models (Pattyn et al., 2013). Although the hysteresis of the GRL-evolution during and after the prescribed boundary-condition perturbation was not as smooth as in most other participating models, the estimated velocities and in particular the expected reversibility of the GRL-position was captured quite well.

6.4 HOM- and FS-solver

The numerical core for HOM-solver is very similar to the original implementation of Pattyn (2003), validated in the the *Ice Sheet Model Intercomparison Project for Higher-Order Models* (ISMIP-HOM) experiments (Pattyn et al., 2008). The FS implementation is basically an extension of this code and has originally been published in Pattyn (2008) for a linear rheology (with $n = 1$ in Eq. 8) and successfully been expanded for nonlinear rheologies (with $n = 3$) by Thoma et al. (2010, 2012). The results of these specific code-fragments are already published, hence we do not present any additional validation of the FS solution here. However, we present a coupled SIA–FS–SSA experiment to demonstrate the flexibility of RIMBAY, with respect of a nested FS-domain within a SIA–SSA domain.

GMDD

6, 3289–3347, 2013

Description of the multi-physics ice flow model RIMBAY

M. Thoma et al.

Title Page

Abstract

Introduction

Conclusions

References

Tables

Figures

◀

▶

◀

▶

Back

Close

Full Screen / Esc

Printer-friendly Version

Interactive Discussion



In this experiment, the bedrock is downward sloping with a central trough

$$B = -100\text{ m} - 1.5x - 300 \cdot e^{-\left(\frac{y-100\text{ km}}{40\text{ km}}\right)^2},$$

the horizontal resolution is 5 km and the accumulation is set to $\dot{m}_{ac} = 0.5\text{ myr}^{-1}$. A Weertman-type sliding law (Eq. 20) is applied as basal boundary condition, modified with an additional basal sliding reduction in the model's domain center according to

$$C = C' \left[1 - 0.5 \exp \left(-\frac{(x - x_j)^2}{2x_j^2} - \frac{(y - y_j)^2}{2y_j^2} \right) \right]$$

with $C' = 10^7\text{ Pa m}^{-1/3}\text{ s}^{1/3}$, $m = \frac{1}{3}$, $x_j = 300\text{ km}$, $x_i = 100\text{ km}$, $y_j = 100\text{ km}$, and $y_i = 10\text{ km}$. (this reduction is similar to those applied in Pattyn et al., 2013). The ice is surrounded by nunataks in the south, west, and north and an ocean in the east. We apply $dS/dx = 0$ at the western ice divide, free slip boundary conditions along the southern and northern nunataks and the dynamic boundary conditions according to Eq. (24) at the ice–ocean boundary. First, the model is run with the coupled SIA–SSA solver and a transition zone of 50 km (applying *schoofism* at the grounding line) until a steady state is reached. Within the transition zone, the SIA and the SSA solutions for the velocity field are interpolated. The final state of this control experiment is shown in Fig. 8a, indicating the ice's geometry as well as the vertically averaged horizontal velocity.

Thereafter, (first) the HOM-solver and (later) the FS-solver are applied to the region, indicated in Fig. 8. As a result the grounding line advantages from 356 km to 398 km (HOM-) and 408 km (FS-solver), respectively, in this synthetic experiment. Pattyn et al. (2012, 2013); Drouet et al. (2013) already discussed the limitations of the SIA/SSA approximations with respect to grounding line migration and pointed out that a high spacial resolution would be necessary to map the whole dynamic behaviour of transient states in ice sheet models.

Description of the multi-physics ice flow model RIMBAY

M. Thoma et al.

Title Page

Abstract

Introduction

Conclusions

References

Tables

Figures

◀

▶

◀

▶

Back

Close

Full Screen / Esc

Printer-friendly Version

Interactive Discussion



However, in ice sheet/ice shelf models on a continental or even global scale and on long time scales (millennia), a high spatial resolution (below 10 km) and a FS-solver, which consumes significant more computational resources than the SIA/SSA approximations, might be too ambitious at present. With respect to the large uncertainties of other atmospheric and ocean modelling issues, like boundary conditions and parameterisations, the drawback of the SIA/SSA approximation might be tolerable for most large scale applications.

7 Conclusions

We have shown, that RIMBAY is capable of reproducing results of previously published experiments and benchmark tests (upper part of Table 2). In addition, RIMBAY has already been successfully applied in many very different scenarios during the last years. These application range from high-resolution FS-modelling of ice flow across subglacial lakes (Thoma et al., 2010, 2012) over studies concerning the interaction between ice sheet, ice shelf and the ocean with a coupled SIA–SSA solver (Determann et al., 2012, 2013; Pattyn et al., 2013), up to coupling RIMBAY with the *Community Earth System Models* (COSMOS) (Barbi et al., 2013) and with *Viscoelastic Lithosphere and Mantle model* (VILMA) (Konrad et al., 2013), which calculates the isostatic adjustment of a spherical earth to (ice-)surface loads.

Two additional modules are implemented within RIMBAY, broadening its versatility: first, the *water layer concept*, developed by (Goeller et al., 2013), providing a sophisticated concept for the evolution of a large-scale subglacial hydrological network, which interacts with the ice sheet by modifying the basal boundary conditions. Second, a sub-grid scale Lagrangian-tracer module, allowing to track tracer propagation through the ice, which assists with the interpretation of the origin and age of ice cores (Sutter et al., 2013). All mentioned applications and modules are summarised in Table 2.

With RIMBAY we provide a scalable open-source ice dynamics model to the scientific community. Based on the specific needs, RIMBAY can be applied easily to new

GMDD

6, 3289–3347, 2013

Description of the multi-physics ice flow model RIMBAY

M. Thoma et al.

Title Page

Abstract

Introduction

Conclusions

References

Tables

Figures

◀

▶

◀

▶

Back

Close

Full Screen / Esc

Printer-friendly Version

Interactive Discussion



scientific issues and is easy extensible because of a well structured interfaces. It provides a broad spectrum of applicability and functionality and could therefore contribute to solve the pressing questions of global climate change.

Appendix A

5 Ice evolution: continuity equation

The finite difference formulation of Eq. (36) for the ice thickness evolution is

$$\begin{aligned}
 & \frac{H^{t+1} - H^t}{\Delta t} - f_{\text{ad}} \frac{D_{j+\frac{1}{2}}(H_{j+1}^{t+1} - H_j^{t+1}) - D_{j-\frac{1}{2}}(H_j^{t+1} - H_{j-1}^{t+1})}{(\Delta x)^2} \\
 & - f_{\text{ad}} \frac{D_{i+\frac{1}{2}}(H_{i+1}^{t+1} - H_i^{t+1}) - D_{i-\frac{1}{2}}(H_i^{t+1} - H_{i-1}^{t+1})}{(\Delta y)^2} \\
 & + (1 - f_{\text{ad}}) \frac{U_{j+\frac{1}{2}}H_{j+\frac{1}{2}}^{t+1} - U_{j-\frac{1}{2}}H_{j-\frac{1}{2}}^{t+1}}{\Delta x} \\
 & + (1 - f_{\text{ad}}) \frac{V_{i+\frac{1}{2}}H_{i+\frac{1}{2}}^{t+1} - V_{i-\frac{1}{2}}H_{i-\frac{1}{2}}^{t+1}}{\Delta y} \\
 & = f_{\text{ad}} \frac{D_{j+\frac{1}{2}}(B_{j+1} - B_j) - D_{j-\frac{1}{2}}(B_j - B_{j-1})}{(\Delta x)^2} \\
 & + f_{\text{ad}} \frac{D_{i+\frac{1}{2}}(B_{i+1} - B_i) - D_{i-\frac{1}{2}}(B_i - B_{i-1})}{(\Delta y)^2} + \dot{m}
 \end{aligned} \tag{A1}$$

where the (diffusive) fluxes $D_{j+\frac{1}{2}} := (D_{j+1} + D_j)/2$ are defined on the edges (half way) between nodes. In Eq. (A1) subscripts ij are omitted if they are constant in a specific

term. The expanded form of is

$$\begin{aligned}
 H^{t+1} - f_{\text{ad}} \frac{\Delta t}{2(\Delta x)^2} & \left[(D_{j+1} + D_j)(H_{j+1}^{t+1} - H_j^{t+1}) - (D_{j-1} + D_j)(H_j^{t+1} - H_{j-1}^{t+1}) \right] \\
 - f_{\text{ad}} \frac{\Delta t}{2(\Delta y)^2} & \left[(D_{i+1} + D_i)(H_{i+1}^{t+1} - H_i^{t+1}) - (D_{i-1} + D_i)(H_i^{t+1} - H_{i-1}^{t+1}) \right] \\
 + (1 - f_{\text{ad}}) \frac{\Delta t}{4\Delta x} & \left[(U_{j+1} + u_j)(H_{j+1}^{t+1} + H_j^{t+1}) - (U_{j-1} + u_j)(H_j^{t+1} + H_{j-1}^{t+1}) \right] \\
 + (1 - f_{\text{ad}}) \frac{\Delta t}{4\Delta y} & \left[(V_{i+1} + v_i)(H_{i+1}^{t+1} + H_i^{t+1}) - (V_{i-1} + v_i)(H_i^{t+1} + H_{i-1}^{t+1}) \right] \\
 = f_{\text{ad}} \frac{\Delta t}{2(\Delta x)^2} & \left[(D_{j+1} + D_j)(B_{j+1} - B_j) - (D_{j-1} + D_j)(B_j - B_{j-1}) \right] \\
 + f_{\text{ad}} \frac{\Delta t}{2(\Delta y)^2} & \left[(D_{i+1} + D_i)(B_{i+1} - B_i) - (D_{i-1} + D_i)(B_i - B_{i-1}) \right] \\
 + (1 - f_{\text{ad}}) \frac{H_{j+1}^t + H_{j-1}^t + H_{i+1}^t + H_{i-1}^t}{4} & + f_{\text{ad}} H^t + M\Delta t
 \end{aligned} \tag{A2}$$

The subscripts $_{ij}$ which doesn't change within a specific term is omitted. The averaging of H^t on the right hand side corresponds to a numerical *Lax scheme* diffusion and stabilises the otherwise unconditional unstable numerical scheme (e.g., Press et al., 2007). Sorting Eq. (A2) with respect to H_{ij}^{t+1} according to the node positions indicated in Fig. 4 and separation of the diffusive and advective parts according to

$$C_i = f_{\text{ad}} C_i^d + (1 - f_{\text{ad}}) C_i^a \tag{A3}$$

GMDD

6, 3289–3347, 2013

Description of the multi-physics ice flow model RIMBAY

M. Thoma et al.

Title Page

Abstract

Introduction

Conclusions

References

Tables

Figures

◀

▶

◀

▶

Back

Close

Full Screen / Esc

Printer-friendly Version

Interactive Discussion



leads to the following coefficients:

$$C_1^d = -\frac{\Delta t}{2(\Delta y)^2} (D_i + D_{i-1})$$

$$C_2^d = -\frac{\Delta t}{2(\Delta x)^2} (D_j + D_{j-1})$$

$$C_3^d = 1 + \frac{\Delta t}{2} \left(\frac{2D_j + D_{j+1} + D_{j-1}}{(\Delta x)^2} + \frac{2D_i + D_{i+1} + D_{i-1}}{(\Delta y)^2} \right)$$

$$5 \quad C_4^d = -\frac{\Delta t}{2(\Delta x)^2} (D_j + D_{j+1})$$

$$C_5^d = -\frac{\Delta t}{2(\Delta y)^2} (D_i + D_{i+1})$$

$$C_1^a = -\frac{\Delta t}{4\Delta y} (V_i + V_{i-1})$$

$$C_2^a = -\frac{\Delta t}{4\Delta x} (U_j + U_{j-1})$$

$$C_3^a = 1 + \frac{\Delta t}{4} \left(\frac{U_{j+1} - U_{j-1}}{\Delta x} + \frac{V_{i+1} - V_{i-1}}{\Delta y} \right)$$

$$10 \quad C_4^a = +\frac{\Delta t}{4\Delta x} (U_j + U_{j+1})$$

$$C_5^a = +\frac{\Delta t}{4\Delta y} (V_i + V_{i+1})$$

$$b_n = f_{\text{ad}} \left[C_2^d (B_j - B_{j-1}) - C_4^d (B_{j+1} - B_j) + C_1^d (B_i - B_{i-1}) - C_5^d (B_{i+1} - B_i) \right] \\ + \frac{1 - f_{\text{ad}}}{4} \left(H_{j-1}^t + H_{j+1}^t + H_{i-1}^t + H_{i+1}^t \right) + f_{\text{ad}} H^t + m \Delta t \quad (\text{A4})$$

GMDD

6, 3289–3347, 2013

Description of the multi-physics ice flow model RIMBAY

M. Thoma et al.

Title Page

Abstract

Introduction

Conclusions

References

Tables

Figures

⏪

⏩

◀

▶

Back

Close

Full Screen / Esc

Printer-friendly Version

Interactive Discussion



These coefficients represent the non-zero elements of a single row n for each ij -element of the matrix \mathbf{A}_{nm} , while b_n represents the right-hand side of Eq. (A2).

Boundary conditions have to be formulated at the edges of the ice body. In case of open boundaries, the unknown value ψ_{i+1} is virtually extrapolated from the interior.

$$5 \quad \psi_{i+1} = 2\psi_i - \psi_{i-1} \quad (\text{A5})$$

An example for the ice thickness H is illustrated in Fig. 9. Substitution of the ice thickness H , the velocity \mathbf{v}_i , the diffusion D_i , and the ice bottom B on the eastern edge according to Eq. (A5) as well as on the southern edge according to $\psi_{j-1} = 2\psi_j - \psi_{j-1}$ in Eq. (A2) results in the highlighted modifications

$$10 \quad \begin{aligned} & H^{t+1} - f_{\text{ad}} \frac{\Delta t}{2(\Delta x)^2} 2(D_j - D_{j-1})(H_j^{t+1} - H_{j-1}^{t+1}) - f_{\text{ad}} \frac{\Delta t}{2(\Delta y)^2} 2(D_{i+1} - D_i)(H_{i+1}^{t+1} - H_i^{t+1}) \\ & + (1 - f_{\text{ad}}) \frac{\Delta t}{4\Delta x} \left[(3U_j - U_{j-1})(3H_j^{t+1} - H_{j-1}^{t+1}) - (U_{j-1} + U_j)(H_j^{t+1} + H_{j-1}^{t+1}) \right] \\ & + (1 - f_{\text{ad}}) \frac{\Delta t}{4\Delta y} \left[(V_{i+1} + V_i)(H_{i+1}^{t+1} + H_i^{t+1}) - (3V_i - V_{i+1})(3H_i^{t+1} - H_{i+1}^{t+1}) \right] \quad (\text{A6}) \\ & = f_{\text{ad}} \frac{\Delta t}{2(\Delta x)^2} 2(D_j - D_{j-1})(B_j - B_{j-1}) + f_{\text{ad}} \frac{\Delta t}{2(\Delta y)^2} 2(D_{i+1} - D_i)(B_{i+1} - B_i) \\ & + f_{\text{ad}} H^t + (1 - f_{\text{ad}}) \frac{0 + H_{j-1}^t + H_{i+1}^t + 0}{1 + 1} + \dot{m} \Delta t \end{aligned}$$

Description of the multi-physics ice flow model RIMBAY

M. Thoma et al.

Title Page

Abstract

Introduction

Conclusions

References

Tables

Figures

◀

▶

◀

▶

Back

Close

Full Screen / Esc

Printer-friendly Version

Interactive Discussion



and consequently in

$$C_1^d = 0$$

$$C_2^d = \frac{\Delta t}{2(\Delta x)^2} 2(D_j - D_{j-1})$$

$$C_3^d = 1 + \frac{\Delta t}{2} \left(\frac{2(D_{j-1} - D_j)}{(\Delta x)^2} + \frac{2(D_{i+1} - D_i)}{(\Delta y)^2} \right)$$

$$5 \quad C_4^d = 0$$

$$C_5^d = \frac{\Delta t}{2(\Delta y)^2} 2(D_i - D_{i+1})$$

$$C_1^a = 0$$

$$C_2^a = -\frac{\Delta t}{4\Delta x} 4U_j$$

$$C_3^a = 1 + \frac{\Delta t}{4} \left(\frac{8U_j - 4U_{j-1}}{\Delta x} + \frac{4V_{i+1} - 8V_i}{\Delta y} \right)$$

$$10 \quad C_4^a = 0$$

$$C_5^a = +\frac{\Delta t}{4\Delta y} 4V_i$$

$$b_n = f_{\text{ad}} \left[C_2^d (B_j - B_{j-1}) - C_5^d (B_{i+1} - B_i) \right] + \frac{1 - f_{\text{ad}}}{2} (H_{j-1}^t + H_{i+1}^t) + f_{\text{ad}} H^t + \dot{m} \Delta t \quad (\text{A7})$$

If the ice adjoins a nunatak, closed boundary conditions are applied. In this case the ice thickness H_{i+1} , the normal velocity $u_{i+\frac{1}{2}}$, and the diffusion $D_{i+\frac{1}{2}}$ vanish in Eq. (33).
 15 Alternatively we can express the unknown value ψ_{i+1} with

$$\psi_{i+\frac{1}{2}} = \frac{\psi_j + \psi_{i+1}}{2} = 0 \quad \text{or}$$

$$\psi_{i+1} = -\psi_j$$

(A8)

Description of the multi-physics ice flow model RIMBAY

M. Thoma et al.

Title Page

Abstract

Introduction

Conclusions

References

Tables

Figures

◀

▶

◀

▶

Back

Close

Full Screen / Esc

Printer-friendly Version

Interactive Discussion



Substituting the ice thickness $H_{j+1} = 0$, the velocity $U_{j+1} = -U_j$, the diffusion $D_{j+1} = -D_j$, and the ice base $B_{j+1} = -B_j$ on the eastern edge as well as $H_{i-1} = -H_i$, $V_{i-1} = -V_i$, $D_{i-1} = -D_i$, and $B_{i-1} = -B_i$ on the southern edge results in the highlighted modifications with respect to Eq. (A2):

$$\begin{aligned}
 & 5 \quad H^{t+1} - f_{\text{ad}} \frac{\Delta t}{2(\Delta x)^2} \left[0 - (D_{j-1} + D_j)(H_j^{t+1} - H_{j-1}^{t+1}) \right] \\
 & \quad - f_{\text{ad}} \frac{\Delta t}{2(\Delta y)^2} \left[(D_i + D_{i+1})(H_{i+1}^{t+1} - H_i^{t+1}) - 0 \right] \\
 & \quad + (1 - f_{\text{ad}}) \frac{\Delta t}{4\Delta x} \left[0 - (U_{j-1} + U_j)(H_{j-1}^{t+1} + H_j^{t+1}) \right] \\
 & \quad + (1 - f_{\text{ad}}) \frac{\Delta t}{4\Delta y} \left[(V_i + V_{i+1})(H_i^{t+1} + H_{i+1}^{t+1}) - 0 \right] \\
 & = f_{\text{ad}} \frac{\Delta t}{2(\Delta x)^2} \left[0 - (D_{j-1} + D_j)(B_j - B_{j-1}) \right] \\
 & \quad + f_{\text{ad}} \frac{\Delta t}{2(\Delta y)^2} \left[(D_i + D_{i+1})(B_{i+1} - B_i) - 0 \right] \\
 & \quad + f_{\text{ad}} H^t + (1 - f_{\text{ad}}) \frac{0 + H_{j-1}^t + H_{i+1}^t + 0}{1 + 1} + \dot{m} \Delta t \tag{A9}
 \end{aligned}$$

Description of the multi-physics ice flow model RIMBAY

M. Thoma et al.

Title Page

Abstract

Introduction

Conclusions

References

Tables

Figures

◀

▶

◀

▶

Back

Close

Full Screen / Esc

Printer-friendly Version

Interactive Discussion



and consequently in

$$C_1^d = 0$$

$$C_2^d = -\frac{\Delta t}{2(\Delta x)^2} (D_{j-1} + D_j)$$

$$C_3^d = 1 + \frac{\Delta t}{2} \left(\frac{D_{j-1} + D_j}{(\Delta x)^2} + \frac{D_j + D_{j+1}}{(\Delta y)^2} \right)$$

$$5 \quad C_4^d = 0$$

$$C_5^d = -\frac{\Delta t}{2(\Delta y)^2} (D_j + D_{j+1})$$

$$C_1^a = 0$$

$$C_2^a = -\frac{\Delta t}{4\Delta x} (U_{j-1} + U_j)$$

$$C_3^a = 1 + \frac{\Delta t}{4} \left(-\frac{U_{j-1} + U_j}{\Delta x} + \frac{V_j + V_{j+1}}{\Delta y} \right)$$

$$10 \quad C_4^a = 0$$

$$C_5^a = +\frac{\Delta t}{4\Delta y} (V_j + V_{j+1})$$

$$b_n = f_{\text{ad}} \left[C_2^d (B_j - B_{j-1}) - C_5^d (B_{j+1} - B_j) \right] + \frac{1 - f_{\text{ad}}}{2} (H_{j-1}^t + H_{j+1}^t) + f_{\text{ad}} H^t + \dot{m} \Delta t \quad (\text{A10})$$

GMDD

6, 3289–3347, 2013

Description of the multi-physics ice flow model RIMBAY

M. Thoma et al.

Title Page

Abstract

Introduction

Conclusions

References

Tables

Figures

◀

▶

◀

▶

Back

Close

Full Screen / Esc

Printer-friendly Version

Interactive Discussion



Appendix B

Velocity: shallow shelf approximation

Reformulating Eq. (16) and sorting with respect to the vertically averaged velocities U and V leads to

$$\begin{aligned} 5 \quad \frac{\partial}{\partial x} \left(4\mu H \frac{\partial U}{\partial x} \right) + \frac{\partial}{\partial y} \left(\mu H \frac{\partial U}{\partial y} \right) - \beta^2 U &= \rho g H \frac{\partial S}{\partial x} - \frac{\partial}{\partial x} \left(2\mu H \frac{\partial V}{\partial y} \right) - \frac{\partial}{\partial y} \left(\mu H \frac{\partial V}{\partial x} \right) \\ \frac{\partial}{\partial y} \left(4\mu H \frac{\partial V}{\partial y} \right) + \frac{\partial}{\partial x} \left(\mu H \frac{\partial V}{\partial x} \right) - \beta^2 V &= \rho g H \frac{\partial S}{\partial y} - \frac{\partial}{\partial y} \left(2\mu H \frac{\partial U}{\partial x} \right) - \frac{\partial}{\partial x} \left(\mu H \frac{\partial U}{\partial y} \right) \end{aligned} \quad (\text{B1})$$

On the Arakawa C-Grid (Fig. 3) the velocities are defined inbetween the thickness (and viscosity) nodes. Defining the increments

$$10 \quad \Delta x_{i,j}^u := 0.5 \cdot \left(\Delta x_{i,j}^H + \Delta x_{i,j+1}^H \right) \quad (\text{B2})$$

$$\Delta y_{i,j}^v := 0.5 \cdot \left(\Delta y_{i,j}^H + \Delta y_{i+1,j}^H \right) \quad (\text{B3})$$

$$\Delta x_{i,j}^* := 0.5 \cdot \left(\Delta x_{i,j}^u + \Delta x_{i+1,j}^u \right) \quad (\text{B4})$$

$$\Delta y_{i,j}^* := 0.5 \cdot \left(\Delta y_{i,j}^v + \Delta y_{i,j+1}^v \right) \quad (\text{B5})$$

Description of the multi-physics ice flow model RIMBAY

M. Thoma et al.

Title Page

Abstract

Introduction

Conclusions

References

Tables

Figures

◀

▶

◀

▶

Back

Close

Full Screen / Esc

Printer-friendly Version

Interactive Discussion



and $\xi := \mu H$ the finite difference version of Eq. (B1) is

$$\begin{aligned}
 & \frac{4\xi_{i,j+1} \frac{U_{i,j+1}-U_{i,j}}{\Delta x_{i,j+1}^h} - 4\xi_{i,j} \frac{U_{i,j}-U_{i,j-1}}{\Delta x_{i,j}^h}}{\Delta x_{i,j}^u} + \frac{\xi_{i+\frac{1}{2},j+\frac{1}{2}}^* \frac{U_{i+1,j}-U_{i,j}}{\Delta y_{i,j}^*} - \xi_{i-\frac{1}{2},j+\frac{1}{2}}^* \frac{U_{i,j}-U_{i-1,j}}{\Delta y_{i-1,j}^*}}{0.5 \left(\Delta y_{i,j}^h + \Delta y_{i,j+1}^h \right)} \\
 & - 0.5 \cdot \left(\beta_{i,j}^2 + \beta_{i,j+1}^2 \right) U_{i,j} \\
 = & \rho g \cdot 0.5 \cdot \left(H_{i,j} + H_{i,j+1} \right) \frac{S_{i,j+1} - S_{i,j}}{\Delta x_{i,j}^u} - \frac{2\xi_{i,j+1} \frac{V_{i,j+1}-V_{i-1,j+1}}{\Delta y_{i,j+1}^h} - 2\xi_{i,j} \frac{V_{i,j}-V_{i-1,j}}{\Delta y_{i,j}^h}}{\Delta x_{i,j}^u} \\
 & - \frac{\xi_{i+\frac{1}{2},j+\frac{1}{2}}^* \frac{V_{i,j+1}-V_{i,j}}{\Delta x_{i,j}^*} - \xi_{i-\frac{1}{2},j+\frac{1}{2}}^* \frac{V_{i-1,j+1}-V_{i-1,j}}{\Delta x_{i-1,j}^*}}{0.5 \left(\Delta y_{i,j}^h + \Delta y_{i,j+1}^h \right)}
 \end{aligned} \tag{B6}$$

$$\begin{aligned}
 & \frac{4\xi_{i+1,j} \frac{V_{i,j+1}-V_{i,j}}{\Delta y_{i+1,j}^h} - 4\xi_{i,j} \frac{V_{i,j}-V_{i,j-1}}{\Delta y_{i,j}^h}}{\Delta y_{i,j}^v} + \frac{\xi_{i+\frac{1}{2},j+\frac{1}{2}}^* \frac{V_{i+1,j}-V_{i,j}}{\Delta x_{i,j}^*} - \xi_{i+\frac{1}{2},j-\frac{1}{2}}^* \frac{V_{i,j}-V_{i-1,j}}{\Delta x_{i,j-1}^*}}{0.5 \left(\Delta x_{i,j}^h + \Delta x_{i+1,j}^h \right)} \\
 & - 0.5 \cdot \left(\beta_{i,j}^2 + \beta_{i+1,j}^2 \right) V_{i,j} \\
 = & \rho g \cdot 0.5 \cdot \left(H_{i,j} + H_{i+1,j} \right) \frac{S_{i+1,j} - S_{i,j}}{\Delta y_{i,j}^v} - \frac{2\xi_{i+1,j} \frac{U_{i+1,j}-U_{i+1,j-1}}{\Delta x_{i+1,j}^h} - 2\xi_{i,j} \frac{U_{i,j}-U_{i,j-1}}{\Delta x_{i,j}^h}}{\Delta y_{i,j}^v} \\
 & - \frac{\xi_{i+\frac{1}{2},j+\frac{1}{2}}^* \frac{U_{i+1,j}-U_{i,j}}{\Delta y_{i,j}^*} - \xi_{i+\frac{1}{2},j-\frac{1}{2}}^* \frac{U_{i+1,j-1}-U_{i,j-1}}{\Delta y_{i,j-1}^*}}{0.5 \left(\Delta x_{i,j}^h + \Delta x_{i+1,j}^h \right)}
 \end{aligned} \tag{B7}$$

Title Page

Abstract

Introduction

Conclusions

References

Tables

Figures

◀

▶

◀

▶

Back

Close

Full Screen / Esc

Printer-friendly Version

Interactive Discussion



with

$$\xi_{i+\frac{1}{2},j+\frac{1}{2}}^* := \frac{1}{4} (\xi_{i,j} + \xi_{i,j+1} + \xi_{i+1,j} + \xi_{i+1,j+1})$$

$$\xi_{i-\frac{1}{2},j+\frac{1}{2}}^* := \frac{1}{4} (\xi_{i,j} + \xi_{i,j+1} + \xi_{i-1,j} + \xi_{i-1,j+1})$$

$$\xi_{i+\frac{1}{2},j-\frac{1}{2}}^* := \frac{1}{4} (\xi_{i,j} + \xi_{i,j-1} + \xi_{i+1,j} + \xi_{i+1,j-1})$$

Defining

$$\alpha_1^u := \frac{\xi_{i,j+1}}{\Delta x_{i,j}^u} \quad \gamma_1^u := \frac{2\xi_{i+\frac{1}{2},j+\frac{1}{2}}^*}{\Delta y_{i,j}^H + \Delta y_{i,j+1}^H}$$

$$\alpha_1^v := \frac{\xi_{i+1,j}}{\Delta y_{i,j}^v} \quad \gamma_1^v := \frac{2\xi_{i+\frac{1}{2},j+\frac{1}{2}}^*}{\Delta x_{i,j}^H + \Delta x_{i+1,j}^H}$$

$$\alpha_2^u := \frac{\xi_{i,j}}{\Delta x_{i,j}^u} \quad \gamma_2^u := \frac{2\xi_{i-\frac{1}{2},j+\frac{1}{2}}^*}{\Delta y_{i,j}^H + \Delta y_{i,j+1}^H}$$

$$\alpha_2^v := \frac{\xi_{i,j}}{\Delta y_{i,j}^v} \quad \gamma_2^v := \frac{2\xi_{i+\frac{1}{2},j-\frac{1}{2}}^*}{\Delta x_{i,j}^H + \Delta x_{i+1,j}^H}$$

the coefficients according to Fig. 10 and the forcing term (on the right hand side) are given by

$$C_3^u = \frac{\gamma_2^u}{\Delta y_{i-1,j}^*}$$

Description of the multi-physics ice flow model RIMBAY

M. Thoma et al.

Title Page

Abstract

Introduction

Conclusions

References

Tables

Figures

◀

▶

◀

▶

Back

Close

Full Screen / Esc

Printer-friendly Version

Interactive Discussion



$$C_4^u = \frac{4\alpha_2^u}{\Delta x_{i,j}^H}$$

$$C_5^u = -\frac{4\alpha_1^u}{\Delta x_{i,j+1}^H} - \frac{4\alpha_2^u}{\Delta x_{i,j}^H} - \frac{\gamma_1^u}{\Delta y_{i,j}^*} - \frac{\gamma_2^u}{\Delta y_{i-1,j}^*} - 0.5 \cdot (\beta_{i,j}^2 + \beta_{i,j+1}^2)$$

$$C_6^u = \frac{4\alpha_1^u}{\Delta x_{i,j+1}^H}$$

$$C_7^u = \frac{\gamma_1^u}{\Delta y_{i,j}^*}$$

$$\begin{aligned} 5 \quad b_m^u &= \rho g \cdot 0.5 \cdot (H_{i,j} + H_{i,j+1}) \frac{S_{i,j+1} - S_{i,j}}{\Delta x_{i,j}^u} \\ &\quad - \frac{2\alpha_1^u}{\Delta y_{i,j+1}^H} (V_{i,j+1} - V_{i-1,j+1}) + \frac{2\alpha_2^u}{\Delta y_{i,j}^H} (V_{i,j} - V_{i-1,j}) \\ &\quad - \frac{\gamma_1^u}{\Delta x_{i,j}^*} (V_{i,j+1} - V_{i,j}) + \frac{\gamma_2^u}{\Delta x_{i-1,j}^*} (V_{i-1,j+1} - V_{i-1,j}) \end{aligned} \quad (B8)$$

$$C_3^v = \frac{4\alpha_2^v}{\Delta y_{i,j}^H}$$

$$C_4^v = \frac{\gamma_2^v}{\Delta x_{i,j-1}^*}$$

$$10 \quad C_5^v = -\frac{4\alpha_1^v}{\Delta y_{i+1,j}^H} - \frac{4\alpha_2^v}{\Delta y_{i,j}^H} - \frac{\gamma_1^v}{\Delta x_{i,j}^*} - \frac{\gamma_2^v}{\Delta x_{i,j-1}^*} - 0.5 \cdot (\beta_{i,j}^2 + \beta_{i+1,j}^2)$$

Description of the multi-physics ice flow model RIMBAY

M. Thoma et al.

Title Page

Abstract

Introduction

Conclusions

References

Tables

Figures

◀

▶

◀

▶

Back

Close

Full Screen / Esc

Printer-friendly Version

Interactive Discussion



$$C_6^v = \frac{\gamma_1^v}{\Delta x_{i,j}^*}$$

$$C_7^v = \frac{4\alpha_1^v}{\Delta y_{i+1,j}^H}$$

$$\begin{aligned}
 b_n^v = & \rho g \cdot 0.5 \cdot (H_{i,j} + H_{i+1,j}) \frac{S_{i+1,j} - S_{i,j}}{\Delta y_{i,j}^v} \\
 & - \frac{2\alpha_1^v}{\Delta x_{i+1,j}^H} (U_{i+1,j} - U_{i+1,j-1}) + \frac{2\alpha_2^v}{\Delta x_{i,j}^H} (U_{i,j} - U_{i,j-1}) \\
 & - \frac{\gamma_1^v}{\Delta x_{i,j}^*} (U_{i+1,j} - U_{i,j}) + \frac{\gamma_2^v}{\Delta x_{i,j-1}^*} (U_{i+1,j-1} - U_{i,j-1})
 \end{aligned} \tag{B9}$$

The lateral boundary condition along the ice shelf front is defined as *free slip*, and hence

$$\frac{\partial U}{\partial y} = 0 \frac{\partial V}{\partial x} = 0 \tag{B10}$$

or

$$\begin{aligned}
 \text{N: } U_{i+1,j} &= U_{i,j} & \Rightarrow \gamma_1^u &= 0 \text{ in } C_7^u \text{ and } C_5^u \\
 \text{S: } U_{i-1,j} &= U_{i,j} & \Rightarrow \gamma_2^u &= 0 \text{ in } C_3^u \text{ and } C_5^u \\
 \text{E: } V_{i,j+1} &= V_{i,j} & \Rightarrow \gamma_1^v &= 0 \text{ in } C_6^v \text{ and } C_5^v \\
 \text{W: } V_{i,j-1} &= V_{i,j} & \Rightarrow \gamma_2^v &= 0 \text{ in } C_4^v \text{ and } C_5^v
 \end{aligned}$$

In case of *no slip* boundary conditions, the flow on the boundary is zero, and hence

$$\frac{u_{i+1,j} + u_{i,j}}{2} = 0 \frac{v_{i+1,j} + v_{i,j}}{2} = 0 \tag{B11}$$

Description of the multi-physics ice flow model RIMBAY

M. Thoma et al.

Title Page

Abstract

Introduction

Conclusions

References

Tables

Figures

◀

▶

◀

▶

Back

Close

Full Screen / Esc

Printer-friendly Version

Interactive Discussion



or

$$N: u_{i+1,j} = -u_{i,j} \quad \Rightarrow \gamma_1^u = 0 \text{ in } C_7^u \text{ and } 2 \text{ in } C_5^u$$

$$S: u_{i-1,j} = -u_{i,j} \quad \Rightarrow \gamma_2^u = 0 \text{ in } C_3^u \text{ and } 2 \text{ in } C_5^u$$

$$E: v_{i,j+1} = -v_{i,j} \quad \Rightarrow \gamma_1^v = 0 \text{ in } C_6^v \text{ and } 2 \text{ in } C_5^v$$

$$5 \quad W: v_{i,j-1} = -v_{i,j} \quad \Rightarrow \gamma_2^v = 0 \text{ in } C_4^v \text{ and } 2 \text{ in } C_5^v$$

Acknowledgements. This work was partly funded by the DFG through grant MA3347/2-1; it was supported by funding from the ice2sea programme from the European Union 7th Framework Programme, grant number 226375; and from the Helmholtz Climate Initiative REKLIM (Regional Climate Change), a joint research project of the Helmholtz Association of German research centres (HGF), which is gratefully acknowledged. The authors wish to thank Sergey Danilov, Angelika Humbert, Thomas Kleiner, Hannes Konrad, Martin Losch, Silvia Massmann, and Johannes Sutter for fruitful discussions.

References

- 15 Arakawa, A. and Lamb, V. R.: Methods of Computational Physics, vol. 17, Academic Press, 1977. 3305
- Barbi, D., Lohmann, G., Grosfeld, K., and Thoma, M.: Ice sheet dynamics within an Earth system model: coupling and first results on ice stability and ocean circulation, Geosci. Model Dev. Discuss., 6, 1–35, doi:10.5194/gmdd-6-1-2013, 2013. 3317, 3337
- 20 Bueler, E., Lingle, C. S., Kallen-Brown, J. A., Covey, D. N., and Bowman, L. N.: Exact solutions and verification of numerical models for isothermal ice sheets, J. Glaciol., 51, 291–306, doi:10.3189/172756505781829449, 2005. 3313, 3337, 3342
- Bueler, E., Brown, J., and Lingle, C.: Exact solutions to the thermomechanically coupled shallow-ice approximation: effective tools for verification, J. Glaciol., 53, 499–516, doi:10.3189/002214307783258396, 2007. 3337
- 25 Church, J. A., Gregory, J. M., White, N. J., Platten, S. M., and Mitrovica, J. X.: Understanding and projecting sea level change, Oceanography, 24, 130–143, doi:10.5670/oceanog.2011.33, 2011. 3290

Description of the multi-physics ice flow model RIMBAY

M. Thoma et al.

Title Page

Abstract

Introduction

Conclusions

References

Tables

Figures

◀

▶

◀

▶

Back

Close

Full Screen / Esc

Printer-friendly Version

Interactive Discussion



- Cuffey, K. M. and Paterson, W. S. B.: The Physics of Glaciers, 4th edn., Elsevier, Oxford, 2010. 3295, 3300
- Determann, J., Thoma, M., Grosfeld, K., and Massmann, S.: Impact of ice shelf basal melting on inland ice-sheet thickness: a model study, *Ann. Glaciol.*, 53, 129–135, doi:10.3189/2012AoG60A170, 2012. 3317, 3337
- Determann, J., Thoma, M., Grosfeld, K., and Hellmer, H.: 21st century ocean warming scenarios: projected loss of grounded ice in the catchment area of Filchner Ronne ice shelves, Antarctica, *The Cryosphere Discuss.*, in preparation, 2013. 3317, 3337
- Docquier, D., Perichon, L., and Pattyn, F.: Representing grounding line dynamics in numerical ice sheet models: recent advances and outlook, *Surv. Geophys.*, 32, 417–435, doi:10.1007/s10712-011-9133-3, 2011. 3308, 3311
- Drouet, A. S., Docquier, D., Durand, G., Hindmarsh, R., Pattyn, F., Gagliardini, O., and Zwinger, T.: Grounding line transient response in marine ice sheet models, *The Cryosphere*, 7, 395–406, doi:10.5194/tc-7-395-2013, 2013. 3316
- Gillet-Chaulet, F., Gagliardini, O., Seddik, H., Nodet, M., Durand, G., Ritz, C., Zwinger, T., Greve, R., and Vaughan, D. G.: Greenland ice sheet contribution to sea-level rise from a new-generation ice-sheet model, *The Cryosphere*, 6, 1561–1576, doi:10.5194/tc-6-1561-2012, 2012. 3291
- Gladstone, R. M., Lee, V., Vieli, A., and Payne, A. J.: Grounding line migration in an adaptive mesh ice sheet model, *J. Geophys. Res.*, 115, F04014, doi:10.1029/2009JF001615, 2010. 3310
- Goeller, S., Thoma, M., Grosfeld, K., and Miller, H.: A balanced water layer concept for subglacial hydrology in large scale ice sheet models, *The Cryosphere Discuss.*, 6, 5225–5253, doi:10.5194/tcd-6-5225-2012, 2012. 3317, 3337
- Greve, R. and Blatter, H.: *Dynamics of Ice Sheets and Glaciers*, *Advances in Geophysical and Environmental Mechanics and Mathematics*, Springer, 2009. 3296, 3298, 3301, 3302
- Hindmarsh, R. C. A. and Payne, A. J.: Time-step limits for stable solutions of the ice-sheet equation, *Ann. Glaciol.*, 23, 74–85, 1996. 3305
- Hooke, R. L.: Flow law for polycrystalline ice in glaciers: comparison of theoretical predictions, laboratory data, and field measurements, *Rev. Geophys. Space Phys.*, 19, 664–672, 1981. 3296
- Huybrechts, P. and Payne, T.: The EISMINT benchmarks for testing ice-sheet models, *Ann. Glaciol.*, 23, 1–12, 1996. 3313, 3337, 3342

Description of the multi-physics ice flow model RIMBAY

M. Thoma et al.

Title Page

Abstract

Introduction

Conclusions

References

Tables

Figures

◀

▶

◀

▶

Back

Close

Full Screen / Esc

Printer-friendly Version

Interactive Discussion



IPCC: The physical science basis, contribution of working group I to the fourth assessment report of the intergovernmental panel on climate change, in: Climate Change 2007, edited by: Solomon, S., Qin, D., Manning, M., Chen, Z., Marquis, M., Averyt, K. B., Tignor, M., and Miller, H. L., Cambridge University Press, Cambridge, UK and New York, NY, USA, 2007. 3290

Jansen, D., Sandhäger, H., and Rack, W.: Model experiments on large tabular iceberg evolution: ablation and strain thinning, *J. Glaciol.*, 51, 363–372, doi:10.3189/172756505781829313, 2005. 3313, 3314, 3337

Joughin, I., Tulaczyk, S., Bamber, J. L., Blankenship, D., Holt, J. W., Scambos, T., and Vaughan, D. G.: Basal conditions for Pine Island and Thwaites Glaciers, West Antarctica, determined using satellite and airborne data, *J. Glaciol.*, 55, 245–257, doi:10.3189/002214309788608705, 2009. 3301

Konrad, H., Thoma, M., Sasken, I., Klemann, V., Grosfeld, K., Barbi, D., and Martinec, Z.: Response of a coupled viscoelastic solid Earth–ice sheet model in peripheral regions, *Surv. Geophys.*, submitted, 2013. 3317, 3337

Levermann, A., Winkelmann, R., Nowicki, S., Fastook, J. L., Frieler, K., Greve, R., Hellmer, H. H., Martin, M. A., Mengel, M., Payne, A. J., Pollard, D., Sato, T., Timmermann, R., Wang, W. L., and Bindshadler, R. A.: Projecting Antarctic ice discharge using response functions from SeaRISE ice-sheet models, *The Cryosphere Discuss.*, 6, 3447–3489, doi:10.5194/tcd-6-3447-2012, 2012. 3291

MacAyeal, D. R.: Large-scale ice flow over a viscous basal sediment: theory and application to Ice Stream B, Antarctica, *J. Geophys. Res.*, 94, 4071–4087, doi:10.1029/JB094iB04p04071, 1989. 3298

Nishida, A.: Experience in developing an open source scalable software infrastructure in Japan, *Lect. Notes Comput. Sc.*, 6017m 87–98, doi:10.1007/978-3-642-12165-4_36, 2010. 3304

Paterson, W. S. B.: *The Physics of Glaciers*, 3rd edn., Butterworth Heinemann, Oxford, 1994. 3295, 3298, 3300, 3302

Paterson, W. S. B. and Budd, W. F.: Flow parameters for ice sheet modeling, *Cold Reg. Sci. Technol.*, 6, 175–177, doi:10.1016/0165-232X(82)90010-6, 1982. 3296, 3313

Pattyn, F.: Ice-sheet modelling at different spatial resolutions: focus on the grounding zone, *Ann. Glaciol.*, 31, 211–216, doi:10.3189/172756400781820435, 2000. 3297

Pattyn, F.: Transient glacier response with a higher-order numerical ice-flow model, *J. Glaciol.*, 48, 467–477, doi:10.3189/172756502781831278, 2002. 3291

Description of the multi-physics ice flow model RIMBAY

M. Thoma et al.

Title Page

Abstract

Introduction

Conclusions

References

Tables

Figures

◀

▶

◀

▶

Back

Close

Full Screen / Esc

Printer-friendly Version

Interactive Discussion



model intercomparison: the effects of thermomechanical coupling, *J. Glaciol.*, 46, 227–238, doi:10.3189/172756500781832891, 2000. 3337

Pollard, D. and DeConto, R. M.: Modelling West Antarctic ice sheet growth and collapse through the past five million years, *Nature*, 458, 329–332, doi:10.1038/nature07809, 2009. 3310

5 Pollard, D. and DeConto, R. M.: Description of a hybrid ice sheet-shelf model, and application to Antarctica, *Geosci. Model Dev.*, 5, 1273–1295, doi:10.5194/gmd-5-1273-2012, 2012. 3310, 3311

Press, W. H., Teukolsky, S. A., Vetterling, W. T., and Flannery, B. P.: *Numerical Recipes: the Art of Scientific Computing*, 3rd edn., Cambridge University Press, New York, NY, USA, 2007. 3304, 3305, 3319

10 Purser, R. J. and Leslie, L. M.: A semi-implicit, semi-Lagrangian finite-difference scheme using high-order spatial differencing on a nonstaggered grid, *Mon. Weather Rev.*, 116, 2069–2080, 1988. 3305

Rahmstorf, S., Foster, G., and Cazenave, A.: Comparing climate projections to observations up to 2011, *Environ. Res. Lett.*, 7, 044035, doi:10.1088/1748-9326/7/4/044035, 2012. 3290

15 Rutt, I. C., Hagdorn, M., Hulton, N. R. J., and Payne, A. J.: The Glimmer community ice sheet model, *J. Geophys. Res.*, 114, 1–22, doi:10.1029/2008JF001015, 2009. 3291

Sandhäger, H.: Quantifizierung eisdynamischer und massenhaushaltsrelevanter Basisgrößen eines antarktischen Inland-Schelfeis-Systems unter Einsatz eines numerischen Fließmodells, Ph. D. thesis, Westfälische Wilhelms-Universität Münster, Münster, Germany, 2000. 3338

20 Schoof, C.: Ice sheet grounding line dynamics: steady states, stability, and hysteresis, *J. Geophys. Res.*, 112, 1–19, doi:doi:10.1029/2006JF000664, 2007. 3310

25 Sutter, J., Lohmann, G., Thoma, M., Barbi, D., and Werner, M.: 3-D tracer advection in polar ice sheets: modeling stratigraphy and isotope distributions in Greenland & Antarctica, Poster, European Geosciences Union, General Assembly, Vienna, Austria, April 2013, EGU2013-10731, 2013. 3317, 3337

Thoma, M., Grosfeld, K., Mayer, C., and Pattyn, F.: Interaction between ice sheet dynamics and subglacial lake circulation: a coupled modelling approach, *The Cryosphere*, 4, 1–12, doi:10.5194/tc-4-1-2010, 2010. 3315, 3317, 3337

30 Thoma, M., Grosfeld, K., Mayer, C., and Pattyn, F.: Ice flow sensitivity to boundary processes: a coupled model study in the Vostok Subglacial Lake area, *Ann. Glaciol.*, 53, 173–180, doi:10.3189/2012AoG60A009, 2012. 3299, 3313, 3315, 3317, 3337

- Van der Veen, C. J. and Whillans, I. M.: Force budget, Part 1: Theory and numerical methods, *J. Glaciol.*, 35, 53–60, doi:10.3189/002214389793701581, 1989. 3296, 3300
- Wessel, P. and Smith, W. H. F.: New, improved version of Generic Mapping Tools released, *Trans. Am. Geophys. U.*, 79, p. 579, doi:10.1029/98EO00426, 1998. 3293, 3312
- 5 Zwinger, T., Greve, R., Gagliardini, O., Shiraiwa, T., and Lyly, M.: A full Stokes-flow thermo-mechanical model for firn and ice applied to the Gorshkov crater glacier, Kamchatka, *Ann. Glaciol.*, 45, 29–37, doi:10.3189/172756407782282543, 2007. 3310

GMDD

6, 3289–3347, 2013

Description of the multi-physics ice flow model RIMBAY

M. Thoma et al.

Title Page

Abstract

Introduction

Conclusions

References

Tables

Figures

⏪

⏩

◀

▶

Back

Close

Full Screen / Esc

Printer-friendly Version

Interactive Discussion



Description of the multi-physics ice flow model RIMBAY

M. Thoma et al.

Title Page

Abstract

Introduction

Conclusions

References

Tables

Figures

⏪

⏩

◀

▶

Back

Close

Full Screen / Esc

Printer-friendly Version

Interactive Discussion

Table 1. List of acronyms.

COSMOS	Community Earth System Models
FS	Full Stokes
gmres	Generalized Minimal RESidual
GRL	grounding line
GMT	Generic Mapping Tools
HOM	Higher Order Model
IPCC	Intergovernmental Panel on Climate Change
ISMIP-HOM	Ice Sheet Model Intercomparison Project for Higher-Order Models
LIS	Library of Iterative Solvers
MISMIP	Marine Ice Sheet Model Intercomparison Project
RIMBAY	R evised I ce M odel B ased on f rAnk p att Y n
SIA	Shallow Ice Approximation
SSA	Shallow Shelf Approximation
UMC	unstable manifold correction
VILMA	Viscoelastic Lithosphere and Mantle model

Description of the multi-physics ice flow model RIMBAY

M. Thoma et al.

Title Page

Abstract

Introduction

Conclusions

References

Tables

Figures

◀

▶

◀

▶

Back

Close

Full Screen / Esc

Printer-friendly Version

Interactive Discussion

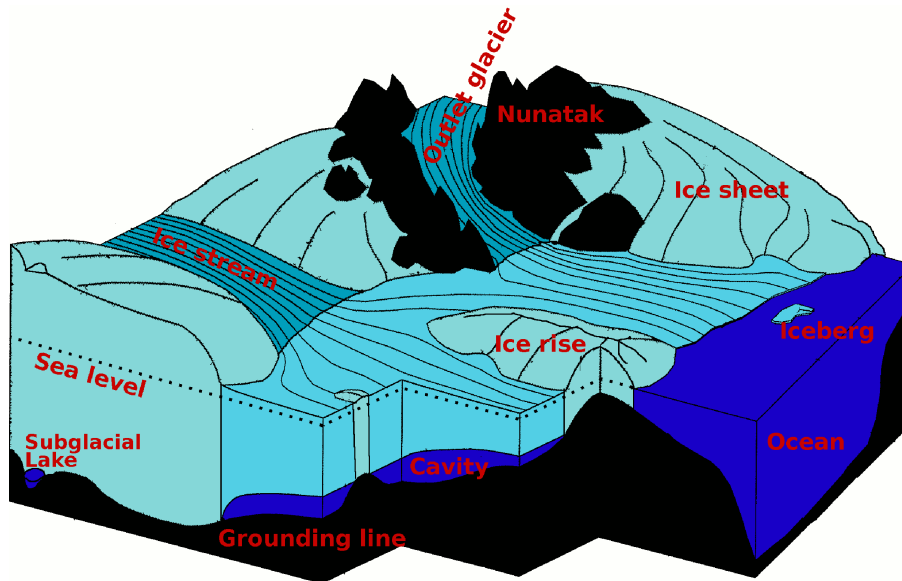


Fig. 1. Sketch illustrating several aspects/components to be considered in ice sheet modelling (adapted after Sandhäger, 2000).

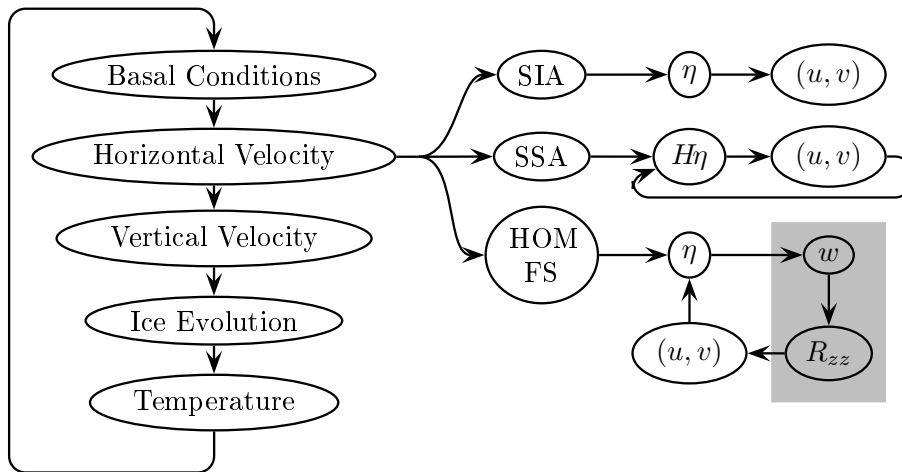


Fig. 2. Sequence of iteratively solved variables within RIMBAY. In the SSA-case the product of $H\eta$ is calculated, instead of the viscosity η , only. The grayish highlighted variables are calculated only in the FS-case.

Description of the multi-physics ice flow model RIMBAY

M. Thoma et al.

Title Page

Abstract Introduction

Conclusions References

Tables Figures

◀ ▶

◀ ▶

Back Close

Full Screen / Esc

Printer-friendly Version

Interactive Discussion



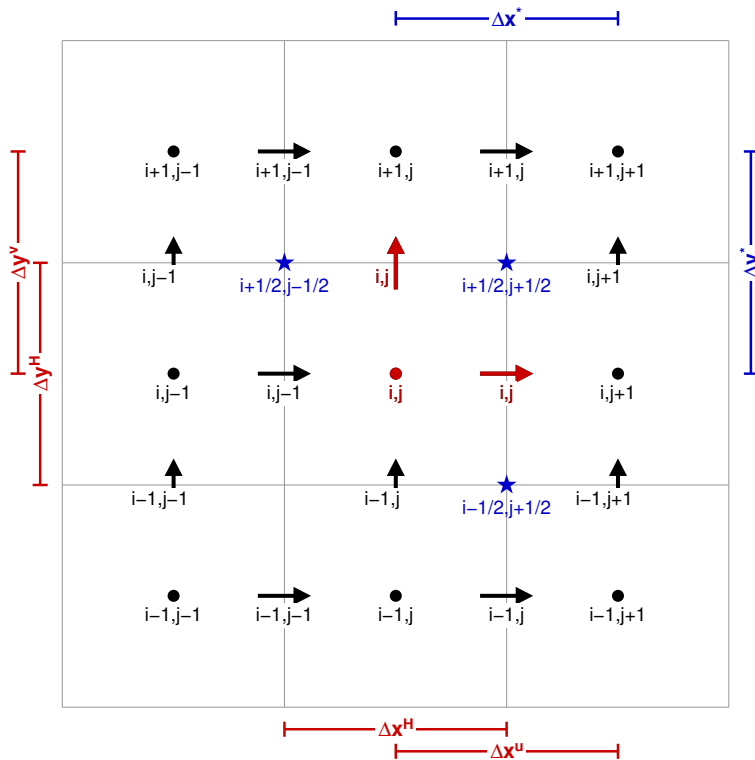


Fig. 3. Location of nodes on a C-Grid. The location of H -, η -, and θ -nodes are indicated by dots while the location of the horizontal velocities are indicated by arrows. The stars indicate certain inter-grid nodes used in the numerical implementation. The red color indicates corresponding nodes of the central i,j -node and the color-coded increments ($\Delta\dots$) at the edges refer to the corresponding grid node distances.

Description of the multi-physics ice flow model RIMBAY

M. Thoma et al.

Title Page	
Abstract	Introduction
Conclusions	References
Tables	Figures
◀	▶
◀	▶
Back	Close
Full Screen / Esc	
Printer-friendly Version	
Interactive Discussion	



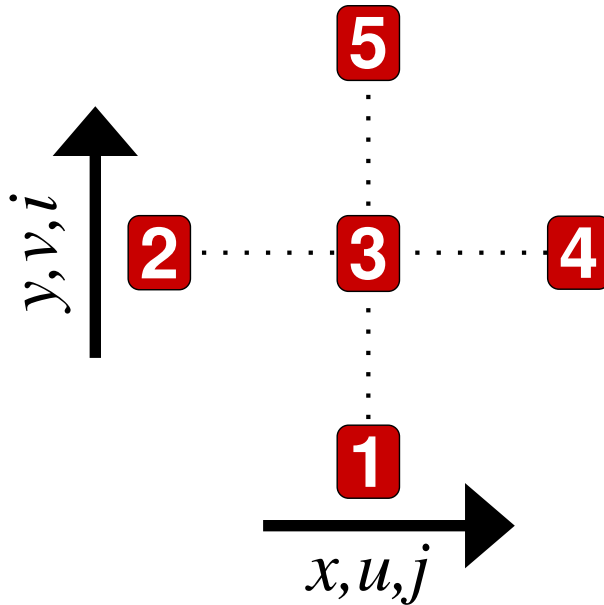


Fig. 4. Relative positions and numbering of nodes for the implicit first order finite difference formulation of the ice evolution (Eq. 30).

Description of the multi-physics ice flow model RIMBAY

M. Thoma et al.

Title Page

Abstract Introduction

Conclusions References

Tables Figures

◀ ▶

◀ ▶

Back Close

Full Screen / Esc

Printer-friendly Version

Interactive Discussion



Description of the multi-physics ice flow model RIMBAY

M. Thoma et al.

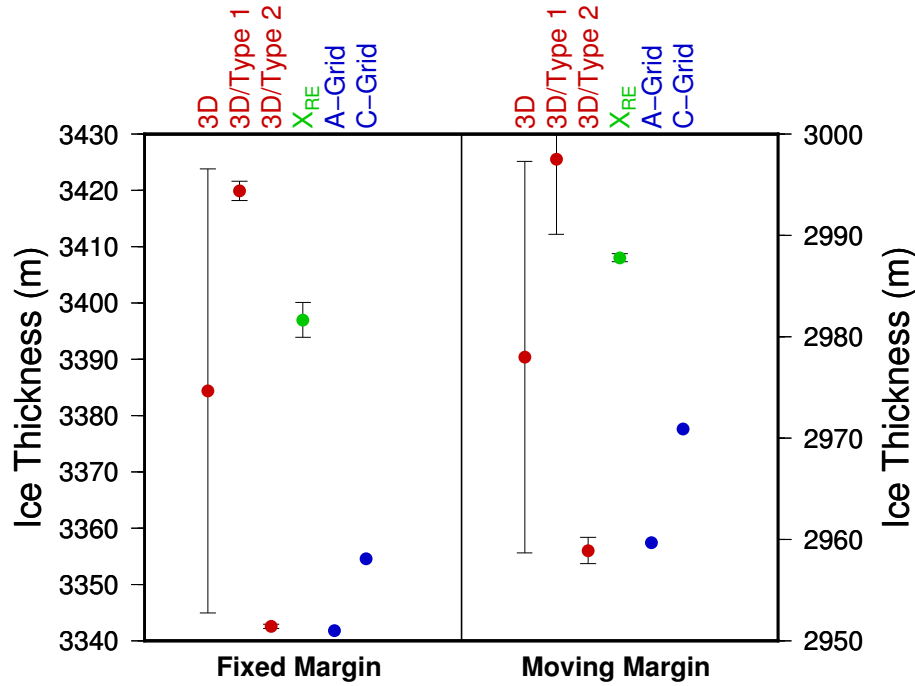


Fig. 5. Comparison of modelled SIA ice thicknesses of experiments described in Huybrechts and Payne (1996) (red), the *Richardson extrapolation* result of Bueller et al. (2005) (green), and RIMBAY results (blue). The RIMBAY A-Grid implementation corresponds essentially with the 3-D/Type-II.

Title Page

Abstract Introduction

Conclusions References

Tables Figures

◀ ▶

◀ ▶

Back Close

Full Screen / Esc

Printer-friendly Version

Interactive Discussion



Description of the multi-physics ice flow model RIMBAY

M. Thoma et al.

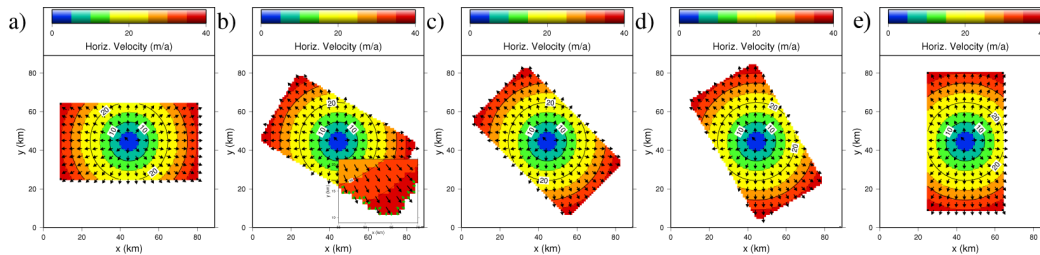


Fig. 6. Modelled horizontal velocity for a synthetic iceberg in different orientations. The enlarged inlet shows exemplarily the orientation of the normal vectors at the ice shelf front in green (compare Eq. 24).

Title Page

Abstract

Introduction

Conclusions

References

Tables

Figures

◀

▶

◀

▶

Back

Close

Full Screen / Esc

Printer-friendly Version

Interactive Discussion



Description of the multi-physics ice flow model RIMBAY

M. Thoma et al.

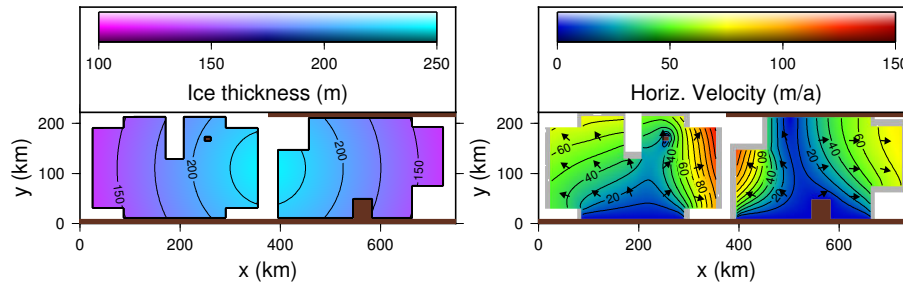


Fig. 7. Modelled horizontal velocity for two synthetic floating ice structures of complex geometries. Nunataks are indicated in brown. At the southern (lower) edge no-slip boundary conditions are applied, at the northern edge and at the ice rise in the left ice body free-slip boundary are valid.

Title Page

Abstract

Introduction

Conclusions

References

Tables

Figures

◀

▶

◀

▶

Back

Close

Full Screen / Esc

Printer-friendly Version

Interactive Discussion



Description of the multi-physics ice flow model RIMBAY

M. Thoma et al.

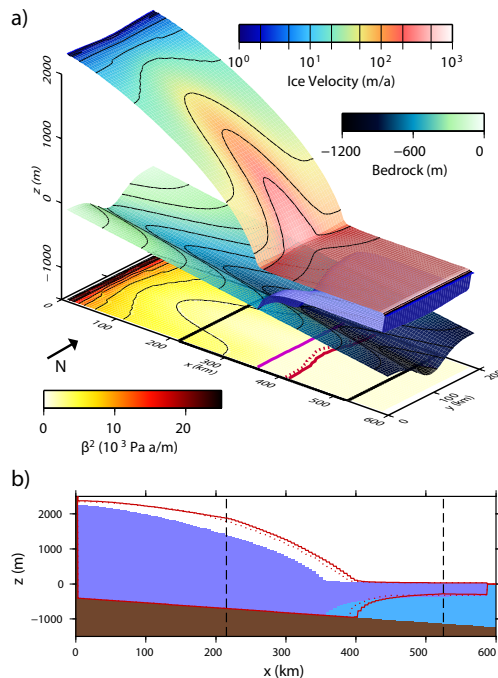


Fig. 8. Geometry for the experiment described in Sect. 6.4. **(a)** Bedrock topography and ice geometry. The horizontal ice velocity is plotted on top of the ice sheet surface; the magenta and red lines indicate the interpolated (sub-grid scale) GRL-positions for the coupled SIA/SSA, the HOM- (dotted) and the FS- (solid) solution, respectively; the black rectangle indicates the region, where the FS-solver is applied. Additionally, the basal friction parameter β^2 (according to Eq. 20) is shown. **(b)** Profile along $y = 100$ km. The dashed black lines indicate the area where the HOM and FS solutions are calculated, respectively; the red lines indicate the shape of the corresponding ice geometry for the HOM-solution (dotted) and FS-solution (solid).

Title Page

Abstract

Introduction

Conclusions

References

Tables

Figures

◀

▶

◀

▶

Back

Close

Full Screen / Esc

Printer-friendly Version

Interactive Discussion



GMDD

6, 3289–3347, 2013

Description of the
multi-physics ice flow
model RIMBAY

M. Thoma et al.

Title Page

Abstract

Introduction

Conclusions

References

Tables

Figures

◀

▶

◀

▶

Back

Close

Full Screen / Esc

Printer-friendly Version

Interactive Discussion

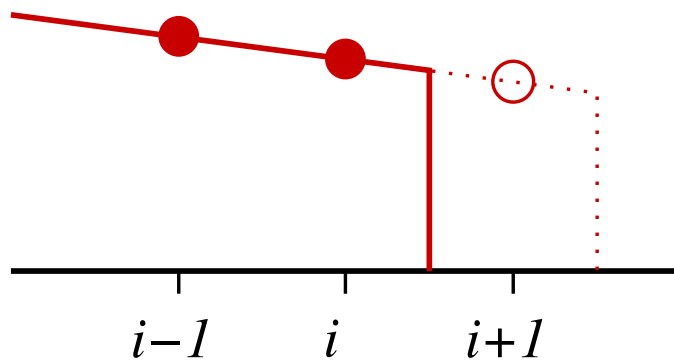


Fig. 9. Extrapolation of ice thickness H at open boundaries.

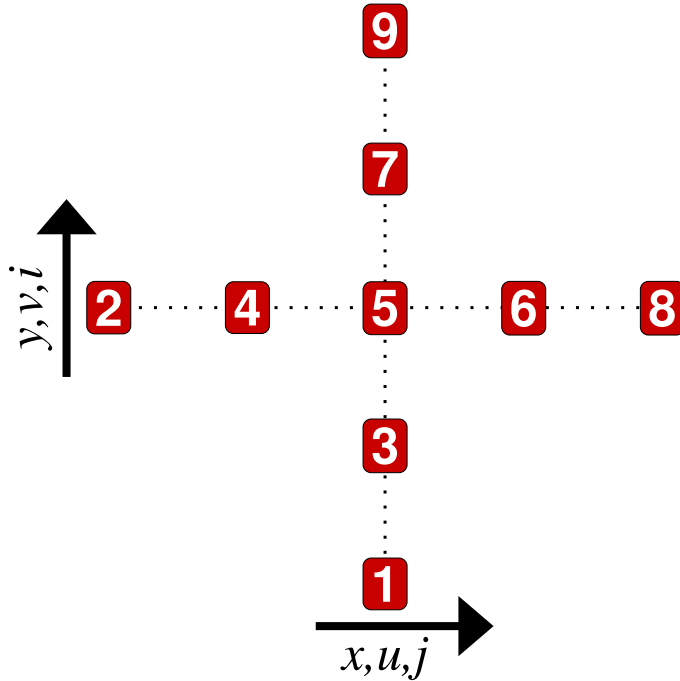


Fig. 10. Relative positions and numbering of nodes for the SSA.

GMDD

6, 3289–3347, 2013

Description of the multi-physics ice flow model RIMBAY

M. Thoma et al.

Title Page

Abstract

Introduction

Conclusions

References

Tables

Figures

⏪

⏩

◀

▶

Back

Close

Full Screen / Esc

Printer-friendly Version

Interactive Discussion

